RESEARCH ARTICLE

The FASEB Journal

White matter hyperintensity genetic risk factor *TRIM47* regulates autophagy in brain endothelial cells

Sunny Hoi-Sang Yeung[1] | Ralph Hon-Sun Lee[1] | Gerald Wai-Yeung Cheng[1] | Iris Wai-Ting Ma[1] | Julia Kofler[2] | Candice Kent[3] | Fulin Ma[3] | Karl Herrup[3] | Myriam Fornage[4] | Ken Arai[5] | Kai-Hei Tse[1,6,7]

[1]Department of Health Technology and Informatics, The Hong Kong Polytechnic University, Kowloon, Hong Kong

[2]Division of Neuropathology, School of Medicine, University of Pittsburgh, Pittsburgh, Pennsylvania, USA

[3]Department of Neurobiology, School of Medicine, University of Pittsburgh, Pittsburgh, Pennsylvania, USA

[4]Human Genetics Center, Division of Epidemiology, School of Public Health, University of Texas Health Science Center at Houston, Houston, Texas, USA

[5]Neuroprotection Research Laboratories, Departments of Radiology and Neurology, Massachusetts General Hospital and Harvard Medical School, Charlestown, Massachusetts, USA

[6]Brain and Mind Centre, University of Sydney, Camperdown, New South Wales, Australia

[7]Department of Neuropathology, Royal Prince Alfred Hospital, Camperdown, New South Wales, Australia

Correspondence
Kai-Hei Tse, Brain and Mind Centre, University of Sydney & Department of Neuropathology, Royal Prince Alfred Hospital, Camperdown, New South Wales, Australia.
Email: kai-hei.tse@sydney.edu.au

Funding information
Hong Kong Polytechnic University (PolyU), Grant/Award Number: P0030307; Leo and Anne Albert Charitable Trust, Grant/Award

Abstract

White matter hyperintensity (WMH) is strongly correlated with age-related dementia and hypertension, but its pathogenesis remains obscure. Genome-wide association studies identified TRIM47 at the 17q25 locus as a top genetic risk factor for WMH formation. TRIM family is a class of E3 ubiquitin ligase with pivotal functions in autophagy, which is critical for brain endothelial cell (ECs) remodeling during hypertension. We hypothesize that TRIM47 regulates autophagy and its loss-of-function disturbs cerebrovasculature.

Abbreviations: 2DG, 2-Deoxy-D-glucose; 3-MA, 3-Methyladenine; AD, Alzheimer's Disease; ATCC, American Type Culture Collection; ATG, Autophagy-related Gene; Atg7, Autophagy-related 7; Baf-A1, Bafilomycin A1; BBB, Blood-Brain Barrier; C-IV, Class IV TRIM Subfamily; DAPI, 4',6-Diamidino-2-Phenylindole; E3, Ubiquitin Ligase Enzyme class E3; ECs, Endothelial Cells; eQTL, Expression Quantitative Trait Locus; FDR, False Discovery Rate; FFPE, Formalin Fixed Paraffin Embedded; GABARAP, Gamma-Aminobutyric Acid Receptor-Associated Protein; GEO, Gene Expression Omnibus; GO, Gene Ontology; GSE, Gene Series Expression (followed by dataset number); GWAS, Genome-Wide Association Studies; HP, Hydrophobic Pocket; HUVEC, Human Umbilical Vein Endothelial Cells; iLIR, Interactive LIR Motif Database; iPSC, Induced Pluripotent Stem Cells; LC3, Microtubule-associated Protein 1A/1B-light Chain 3; LC3B I, Microtubule-associated Protein 1A/1B-light Chain 3 Beta (form I); LC3B II, Microtubule-associated Protein 1A/1B-light Chain 3 Beta (form II); LIR, LC3-Interacting Region; MCAO, Middle Cerebral Artery Occlusion; MRI, Magnetic Resonance Imaging; NCBI, National Center for Biotechnology Information; p62, Sequestosome 1 (also known as SQSTM1); PAGE, Polyacrylamide Gel Electrophoresis; PAH, Pulmonary Arterial Hypertension; PBS, Phosphate Buffered Saline; PDB, Protein Data Bank; PSSM, Position Specific Scoring Matrix; p-ULK1, Phosphorylated Unc-51 Like Autophagy Activating Kinase 1; Rapa, Rapamycin; RING, Really Interesting New Gene (domain); scRNAseq, multiple single cell RNAseq; SIM, Structured Illumination Microscopy; siRNA, Small Interfering RNA; SNP, Single Nucleotide Polymorphism; SQSTM1, Sequestosome 1 (also known as p62); TFEB, Transcription Factor EB; TRIM, Tripartite Motif; ULK1, Unc-51 Like Autophagy Activating Kinase 1; V-ATPase, Vacuolar ATPase; WMH, White Matter Hyperintensity; WT, Wildtype; xLIR, Extended LC3 Interacting Region.

Based on transcriptomics and immunohistochemistry, TRIM47 is found highly expressed by brain ECs in human and mouse, and its transcription is upregulated by artificially induced autophagy while downregulated in hypertension-like conditions. Using in silico simulation, immunocytochemistry and super-resolution microscopy, we predicted a highly conserved binding site between TRIM47 and the LIR (LC3-interacting region) motif of LC3B. Importantly, pharmacological autophagy induction increased Trim47 expression on mouse ECs (b.End3) culture, while silencing *Trim47* significantly increased autophagy with ULK1 phosphorylation induction, transcription, and vacuole formation. Together, we demonstrate that TRIM47 is an endogenous inhibitor of autophagy in brain ECs, and such TRIM47-mediated regulation connects genetic and physiological risk factors for WMH formation but warrants further investigation.

KEYWORDS

autophagy, brain endothelial cells, TRIM family, *TRIM47*, white matter hyperintensity

1 | INTRODUCTION

White matter hyperintensities (WMH) are abnormally strong signals detectable by magnetic resonance imaging (MRI) commonly found in the aging brain. The intense signals of WMH are the likely consequence of cerebrovascular changes with freely diffusible fluid originating from a leaky blood–brain barrier (BBB), microbleeds.[1,2] The age-related WMH burden increases with age and is significantly associated with cognitive decline.[3–7] The radiopathological correlation studies of WMH regions revealed a range of neuropathology including microinfarcts, astrogliosis, microglia activation, arteriolosclerosis, and myelin loss.[8–11] The most consistent is BBB leakage as evidenced by the detection of fibrinogen in the penumbra region.[12,13] At the WMH site, the cerebral capillary dysfunction triggers blood flow reduction, and BBB disruption followed by fibrinogen breaching which ultimately causes oligodendrocyte loss.[14] While the gradual myelin loss would lead to cognitive impairment in age-related dementia,[15] the initial mechanism triggering the cerebrovascular changes underlying the WMH formation remains elusive.

Hypertension is one of the most prevalent conditions in the aging population, and it is the major risk factor for WMH formation.[16–18] The chronic hardening and narrowing of blood vessels in the cerebrovasculature can drive WMH-associated cognitive impairment even in young and asymptomatic populations.[19,20] Cerebrovasculature is a highly dynamic system, whose flexibility is conferred by the constituent endothelial cells (ECs).[21] EC is the main cellular constituent of BBB, which forms the interface between blood and brain and under the regulation of astrocytes and pericytes.[22] At the vascular lumen, ECs constantly encounter shear stress of blood flow and adapt to hemodynamics by remodeling themselves through autophagy.[23,24] In hypertensive conditions, the vascular tone and blood flow in the cerebrovasculature are impaired,[25] and likely lead to autophagy failure in ECs.[26,27] As the restoration of autophagy was shown to reduce hypertension-associated cerebrovascular dysfunction,[28] we propose that impaired autophagy in ECs may be the underlying cause of hypertension-driven BBB leakage and WMH formation.

Despite the link between hypertension, autophagy failure, and BBB leakage, not every hypertensive patient develops WMH.[17] Population genetics fill this gap of knowledge. Independent genome-wide association studies (GWAS) identified single nucleotide polymorphism (SNPs) that confer significant risk to WMH development in the healthy aging population at locus at 17q25.[29–34] Among the six genes (*WBP2, TRIM65, TRIM47, MRPL38, FBF1*, and *ACOX1*) found at this locus, two are members of the tripartite motif (TRIM) family. Importantly, a recent study combining GWAS and whole exome sequencing mapped to a missense variant of *TRIM47* that may cause damaging effects toward WMH formation.[35] TRIM is a large family of E3 ubiquitin ligases with more than 80 members in the human genome. Members of the TRIM family regulate protein turnover, quality control, and degradation through the ubiquitin-proteasome system during development, immunity, and carcinogenesis.[36] Surprisingly, TRIM family members are also heavily involved in the regulation of autophagy.

Many TRIM members were experimentally verified to interact with key autophagic adaptors including LC3, SQSTM1/p62, or ULK1/Beclin. Together, the proteins form a TRIM-containing complex during autophagosome formation for macroautophagy,[37] as well as selective microautophagy to precisely degrade intracellular organelles.[38] For example, TRIM65 is known to facilitate autophagy by controlling Atg7 expression in cancer cells.[39] Yet, the role of TRIM47 in autophagy remains unknown, especially in the endothelium. With the strong population genetic evidence, we propose that the dysfunction of TRIM47 may cause autophagy failure in brain ECs, followed by BBB disintegration and WMH formation. In this study, we test our hypothesis by characterizing the endpoint changes of TRIM47 using a series of bioinformatic analyses in silico coupled with a cell biology experiment of TRIM47 in EC autophagy and in vitro.

2 | METHODS

2.1 | Query of gene expression omnibus repository and scRNA-seq

The Gene Expression Omnibus (GEO) repository of NCBI was queried for datasets targeting hypertension, autophagy, and/or endothelial cells. Four datasets (GSE108384, GSE199709, GSE180169, and GSE131712) were identified to test our hypothesis that *TRIM47* expression is altered in endothelial cells in hypertensive environments. The exploration and re-analysis were performed on the GEO2R R-based web application[40] and GREIN:GEO RNA-seq Experiments Interactive Navigator.[41] The differential gene expression signature obtained in the pairwise comparison was identified. The significantly upregulated or downregulated genes reaching a false discovery rate or an adjusted p-value <.05 were then curated for gene ontology (GO) enrichment analysis by a PANTHER-based platform.[42]

2.2 | In silico analysis of TRIM47

To screen for the LC3-interacting region (LIR) motif among the protein sequences of TRIM family members, we queried the iLIR database, a web-based search engine for LIR motif-containing proteins in eukaryotes.[43,44] To simulate the three-dimensional structure, the protein sequence of TRIM47 was mapped using Phyre2 server as described.[45] The best-fit model generated by Phyre2, as well as the human and mouse TRIM47 protein model predicted by Alphafold artificial intelligence algorithm[46] were docked with the human (PDB: 3VTU) or mouse

LC3B (Alphafold: Q8C0E3) models using ClusPro web server 2.0.[47] The computed binding affinity between the protein structures was sorted based on scores measured by the estimated free energy coefficient ($E_{balanced}$) and the binding cluster size. The best-ranked protein–protein interaction structures were then explored, annotated, and analyzed for contact area using the software ICM Browser Pro (Molsoft L.L.C.).[48]

2.3 | Postmortem human brain tissue

A cohort of formalin-fixed paraffin-embedded postmortem brain tissues was used were kindly provided by the Neuropathology Core of Alzheimer's Disease Research Center at University of Pittsburgh Medical Center with approvals from the Committee for Oversight of Research and Clinical Training Involving Decedents at University of Pittsburgh. The postmortem tissues were of frontal cortex origin (Brodmann area 9) from two males and seven females of Alzheimer's disease (AD, Braak Stage VI) and age-matched controls (Braak Stages 0–III) between the ages of 73 and 90 years old. The postmortem interval was between 3.5 and 19 h. All tissues were sectioned at 12 μm and stored at room temperature until use.

2.4 | Animal study

The animal experiment was approved by the Animal Subjects Ethics Sub-Committee at The Hong Kong Polytechnic University (PolyU) (ASESC Case No.: 20-21/167-HTI-R-GRF) with a valid license from the Department of Health in Hong Kong. Wildtype mice (WT, C57BL/6J) were housed in individually ventilated cages (Techniplast, Italy) in a temperature and humidity-controlled environment with food (PicoLab Diet 5053, LabDiet Inc, MO, USA) and water ad libitum on a 12-h light/dark cycle The brain tissue was extracted from WT mice at 10 months of age ($n=3$). Briefly, animals were deeply anesthetized prior to transcardial perfusion with phosphate buffer saline, as described earlier.[49] The fresh brain was fixed by paraformaldehyde (4%, 24 h) and then cryoprotected in phosphate buffer saline (PBS)-sucrose (30% w/v, 72 h) at 4°C before embedded for cryosectioning on SuperFrost-plus slides at 10 μm thickness.

2.5 | Immunohistochemistry–immunofluorescence

For human tissue, the paraffin-fixed sections were dewaxed with xylene before rehydration in a series of

ethanol/phosphate-buffered saline. The rehydrated sections were antigen retrieved with citrate buffer (pH 6.0) at 95°C for 10 min. After cooling and rinsing, the nonspecific antibody binding was then blocked using 10% donkey serum at room temperature for 1 hour, followed by overnight incubation at 4°C with the primary antibody against TRIM47 (1:100, rabbit polyclonal, ab72234, Abcam). The tissue sections were washed and then incubated in AlexaFluor-conjugated secondary antibody for 1 h at room temperature with nuclear counterstained by PI. All immunofluorescence image of the human tissues was captured at University of Pittsburgh using a Nikon A1R confocal system based on an Eclipse Ti2 microscope equipped with a 20× (Nikon N Plan Apo 20x/0.75), 40× (Nikon N Plan Apo 40x/0.95) dry objectives, or 60× (1.4 Numerical Aperture) oil objective lens and a camera (at $512\,\mu m \times 512\,\mu m$) operated by NIS-Elements AR software. Three Region-Of-Interests were captured per specimen for quantification.

For mouse tissue, the frozen sections were washed and blocked with normal donkey serum (10% v/v) in PBS with 0.3% Triton X-100 for 1 h at room temperature. Then blocked tissues were then incubated with specific primary antibodies against anti-CD31 antibody [P2B1] ab24590 (1:500, mouse monoclonal, ab72234, Abcam) and anti-TRIM47 (1:500, rabbit polyclonal, ab72234, Abcam) overnight at 4°C. The sections were then washed with PBS before incubation with incubated secondary antibodies against mouse or rabbit IgG conjugated with Alexa Fluor 488 or 555 or 647 (Thermo Fisher Scientific, MA) for 1 h at room temperature. All nuclei were counterstained with DAPI before mounting in Hydromount (National Diagnostics, GA, USA) with coverslips. Whole brain tissue sections were taken by a Nikon Eclipse Ti2-E Live-cell Fluorescence Imaging System at University Research Facility in Life Sciences as described below. The image was analyzed by ImageJ (FIJI 1.53, National Institute of Health, MD, USA).

2.6 | Cell culture study

To study the function of Trim47 in autophagy, an endothelial cell line derived from mouse brain, bEnd.3 (CCL-2299, ATCC), was used.[50] bEnd.3 cells were maintained in complete Dulbecco's Modified Eagle Medium supplemented with 10% (v/v) fetal bovine serum and 1% (v/v) and penicillin/streptomycin mixture in the incubator at 37°C with 5% CO_2. To passage, the cells were detached with 0.25% (v/v) trypsin before replating. To study autophagy, bEnd.3 cells were treated with either 3-methyladenine (3-MA, #1292 Tocris, MN, USA) or rapamycin (Rapa, #3977 Tocris, MN, USA) or Bafilomycin A1 (Baf-A1, #1334 Tocris, MN, USA)

for 24 h, or gene silencing described below, before downstream analysis.

2.7 | Gene silencing

To study the loss-of-function, *Trim47* expression in bEnd.3 cells was silenced by SMARTpool siRNA (siGENOME Mouse Trim47, Gene ID 217333, M-056879-01-0020) or control siRNA (siGENOME non-targeting, D-001206-13-20) using DharmaFECT 1 Transfection Reagent (T-2001-02, Horizon Discovery, USA) according to manufacturer's instruction.

2.8 | Western blotting

To obtain cell lysates, the cells were lysed in radioimmunoprecipitation assay buffer (20–188, Millipore, CA, USA) with protease and phosphatase inhibitors (Roche, Hong Kong). After quantification, the protein samples were normalized (Bio-Rad Protein Assay, 5000001, Bio-Rad, CA, USA) and 30 μg were loaded into a 7.5 to 12% sodium dodecyl sulfate (SDS)–polyacrylamide gel for electrophoresis. For the routine immunoblotting, the protein was heated for 5 min at 95°C for denaturation. For non-denaturing immunoblotting, the heating step was omitted and the SDS was omitted from the sample buffer. The resolved proteins were transferred to a semi-dry polyvinylidene difluoride membrane using a Bio-Rad Trans-Blot Turbo Transfer System (1 704 150, Bio-Rad, CA, USA). After blocking non-specific bindings with 5% non-fat milk, the blot was probed against TRIM47 (1:500, rabbit polyclonal, ab72234, Abcam), LC3B (1:1000, E5Q2K, mouse monoclonal #83506, Cell signaling technology/CST), ULK1 (1:1000, D8H5, rabbit monoclonal #8054S, CST), p-ULK (Ser555) (1:1000, D1H4, rabbit monoclonal, #5869, CST), p62 (1:1000, D1Q5S, rabbit monoclonal, #39749, CST), p-p62 (Ser349) (1:1000, E7M1A, rabbit monoclonal, #16177, CST), and GABARAP (1:1000, E1J4E, rabbit monoclonal, #13733, CST). After overnight incubation, the probed blots were incubated with horseradish peroxidase-conjugated secondary immunoglobulins (Cell Signaling Technology, MA, USA). After washes with tris-buffer saline-Tween, the protein signals were captured by chemiluminescent substrates (SuperSignal™ West Pico or Extended Dura or Femto Maximum Sensitivity Substrate, Thermo Fisher Scientific, MA, USA) and the blot image was acquired using Bio-Rad ChemiDoc MP Imaging System (12003154, Bio-Rad, CA, USA) with a continuous exposure for 5 min. To quantify the protein expression level, the density and the size in kilodalton (kDa) of each

individual band were measured by ImageJ (FIJI, v1.53, National Institute of Health, MD, USA).

2.9 | Gene expression

The total RNA was isolated from the cells using the RNeasy Mini Kit (Qiagen, Germany, 74106). Any remaining genomic DNA in the RNA sample was digested by DNase I (1 Unit /μL, Thermo Fisher Scientific, MA, USA). To generate cDNA, reverse transcription was performed with a high-capacity RNA-to-cDNA kit (Applied Biosystem, Thermo Fisher Scientific, MA, USA). The genes of interest and the housekeeping gene, *Gapdh*, were amplified and analyzed in real-time polymerase chain reaction on a Roche Light Cycler 480 system with TB Green® Premix Ex Taq™ II (TaKaRa Bio Inc., Japan). The specific primers were predesigned and validated by PrimerBank of Massachusetts General Hospital,[51] with the primer sequences detailed in Table S1.

2.10 | Immunocytochemistry

For microscopic examination, immunocytochemistry was performed as described.[49] The bEnd.3 cells plated on coverslips were fixed by 4% paraformaldehyde (pH 7.2) for 30 min. After washing with PBS, the potential non-specific binding was blocked with 5% (v/v) normal donkey serum (D9663, Sigma–Aldrich) in PBS containing 0.3% Triton X-100 for 30 min at room temperature. The specimen was then incubated with primary antibody against LC3B (83506S, 1:400, Cell Signaling Technology) as well as TRIM-47 (ab72234, 1:400, Abcam), p-p62 Ser349 (1:800, CST, #16177S), p-ULK1 Ser555 (1:250, CST, #5869), or GABARAP (1:200, CST, #13733) for 2 h, followed by fluorescent visualization with donkey anti-mouse or anti-rabbit Alexa fluor-488 or −555 (A31572, A21202, Thermo Fisher Scientific, MA, USA). The stained coverslip was further incubated with DAPI (4′,6-diamidino-2-phenylindole, 1 μg/mL) for 5 min before being mounted on a glass slide with Hydromount aqueous mounting medium (HS106100ML, National Diagnostics). The coverslips were examined with a Nikon Eclipse Ti2-E Live-cell Fluorescence Imaging System at University Research Facility in Life Sciences. The system is equipped with DS-Qi2 monochrome camera and a multi-wavelength LED illumination system (CoolLED pE-4000) with blue (Ex: 380/55), green (Ex: 470/30), red (Ex: 557/35), and far-red (Ex: 620/60) filters with a Nikon Plan Apo λ 20x Objective (N.A. 0.75, R.I. 1.0). Duplicate coverslips were included for each condition and a total of five images (2424 × 2424 pixel) from random fields (882.5 μm × 882.5 μm) was acquired using Nikon

NIS elements software, (V5.21.03 Nikon Instruments, NY, USA). Image analysis was performed by QuPath[52] and Cellprofiler.[53]

2.11 | Quantification of autophagic puncta

The quantification of ATG8 puncta is a standard approach to measuring the level of autophagic flux.[54] To quantify autophagy, the immunocytochemistry image was analyzed by the open-source CellProfiler Software of version 4.2.5.[53] Briefly, the triple immunofluorescent images (2424 × 2424 pixels at 0.36 μm/pixel) were separated into three channels and converted into greyscale. The primary objects of the nucleus, green or red puncta were identified and related in each cell. The related features were then classified, filtered, and masked for the measurement of signal colocalization. In each masked cell, the second and tertiary objects segmenting the cytoplasm and the cytoplasmic puncta were then identified and classified, with the number of cytoplasmic puncta in each positive cell quantified for analysis.

2.12 | Structured illumination microscopy imaging

Super-resolution microscopy was performed using a structured illumination microscopy (SIM) system at University Research Facility in Life Sciences. The Nikon N-SIM was built on a fully motorized Eclipse Ti inverted microscope body equipped with Nikon LU-NV MultiLaser (TIRF), ORCA-Flash4.0 V2+ sCMOS camera, and CFI SR HP Plan Apo 100× (NA = 1.35) oil objective lens. The XY resolution is 115 nm and the Z resolution is 250 nm in SIM mode (Nikon Instruments, NY, USA). To prepare the samples for N-SIM, cells were plated on 1.5H 13 mm Marienfeld no. round coverglass as described above but with the specimen mounted using ProLong Diamond antifade mountant (Thermo Fisher Scientific, MA, USA). The acquired datasets with an array of 1024 × 1024 pixels across the Z steps of 1 micron were computationally reconstructed using the built-in algorithm in NIS-Elements AR software. To evaluate the puncta colocalization, the images were analyzed using the BIOP-JACoP (*Just another colocalization*) plugin in ImageJ in accordance with earlier guidelines.[55,56] Briefly, the Costes′ randomization analysis, Pearson′s coefficient, and Manders′ overlap coefficient (M1 = summed intensities of pixels from the TRIM47 (green) signal in which the intensity of LC3 (red) is above zero; M2 = summed intensities of pixels from the LC3 (red) signal in which the intensity of TRIM47 (green)

is above zero) were employed as measurement of colocalization, as described previously.[57]

2.13 | Statistics

For each experiment, at least three independent biological replicates were included, and the total number of experiments is denoted as *n* number in each graph. A Grubbs test was performed to identify outliners identification.[58] For comparisons of one variable between two groups, an unpaired *t*-test was performed. For comparisons of one variable in more than two groups, a one-way analysis of variance (ANOVA) was performed with post-hoc tests for multiple comparisons. For comparisons of two or more variables in two groups or more, a two-way ANOVA with a post-hoc multiple comparison was conducted. All statistical analyses were performed using GraphPad Prism software version 10.0 (GraphPad Software Inc. MA, USA). All statistical analyses were two-tailed, and the significance level was set at $p < .05$. The details of the analysis and post-hoc tests are stated in each figure legend.

3 | RESULTS

To test our hypothesis that TRIM47 dysfunction in the brain endothelium leads to WMH formation, we first sought to demonstrate if *TRIM47* was highly expressed in brain EC. We queried multiple single-cell RNAseq (scRNAseq) database of human and mouse brain tissues using the single-cell portal (Figure 1). In two independent scRNAseq libraries of human prefrontal cortices from healthy adult subjects,[59,60] *TRIM47* expression was highly enriched in the brain ECs and astrocytes and essentially absent in neurons and other brain cell types (Figure 1A). Further exploration of an additional scRNAseq library of normal human BBB further showed that brain ECs from arterioles, capillaries, and veins similarly express TRIM47 and their level is stronger than that of pericytes and fibroblast (Figure 1B,C),[61] while the level in smooth muscle cells was highly variable. To examine *Trim47* expression pattern in the mouse brain, we explored the scRNAseq library of the mouse whole brain (C57BL/6J, 2–3 months of age, $n = 8$),[62] and a scRNAseq library of the mouse whole cerebral cortex (C57BL/6J, 1 month of age, $n = 1$).[63] We found that *Trim47* is strongly expressed by mouse brain ECs in these independent libraries (Figure 1D). This is agreed by an additional query on a third library of scRNAseq of transcriptions from nine adult mouse brain regions (i.e., frontal cortex, posterior cortex, substantia nigra, striatum, thalamus, globus pallidus, entopeduncular, hippocampus, and cerebellum; C57Blk6/N, 2 months of age).

In each brain region, the highest level of *Trim47* transcription was found in the Flt1+ ECs population (Figure 1E, http://dropviz.org/).[64] In all datasets, astrocytes, pericytes, and vascular smooth muscle cells also express *TRIM47*, but only ECs consistently and highly expressed in both human and mouse. These observations from six independent scRNAseq datasets agree with our histology experiments. Using immunohistochemistry on a cohort of healthy and AD human cerebral cortex, we found that TRIM47 signals are detectable in the endothelium of the capillary and arteriole-like structures, but not in neuron or neuropil (Figure 2A,B). In wild-type C57BL/6J mice at 10 months old, we also observed that Trim47 is highly expressed by CD31+ brain endothelial cells in both male and female brains (Figure 2C).

As autophagy regulates von Willebran factor and upregulates nitric oxide release in ECs[23,24] and the high laminar shear stress on the endothelium by the physiological blood flow activates autophagy in Ecs,[26] autophagy is an important mechanism for remodeling the vascular structure to adapt hemodynamics. We therefore characterized *TRIM47* expression in ECs during autophagy and autophagy-inducing conditions through a meta-analysis of TRIM family members in independent RNA-seq datasets. First, in adenovirus-mediated TFEB (transcription factor EB, the master regulator of autophagy) overexpression in primary human EC culture (HUVEC, human umbilical vein endothelial cells), autophagy was significantly induced with increased EC migration and tube formation.[65] The meta-analysis of the microarray dataset (GSE108384) showed that 27 *TRIM* family members were significantly and differentially expressed in these autophagic human ECs (adjusted *p* value <.05). Among the differentially expressed *TRIM* members, *TRIM47* was the third most upregulated gene (Log_2 fold change = 1.16, Figure 3A). To test our hypothesis that TRIM47 function may be associated with such blood flow-related autophagy, we inquired *TRIM* family member's expression in a human aortic ECs model with or without luminal shear stress simulation ($12\,dyn/cm^2$, 12 h; RNA-seq, GSE199709).[66] In gene ontology analysis, macroautophagy (GO:0034262) was significantly enriched by the differentially upregulated genes expressed by ECs immediately after 12 h of shear stress treatment. In this autophagic condition, 14 out of the 49 detectable *TRIM* family members were significantly and differentially expressed by the ECs, where *TRIM47* was the sixth most significantly downregulated family member (Log_2 fold change = −0.41, Figure 3B), but such reduction was abolished after 24 h of recovery in static medium. The details of these re-analyses can be found in Tables S2 and S3.

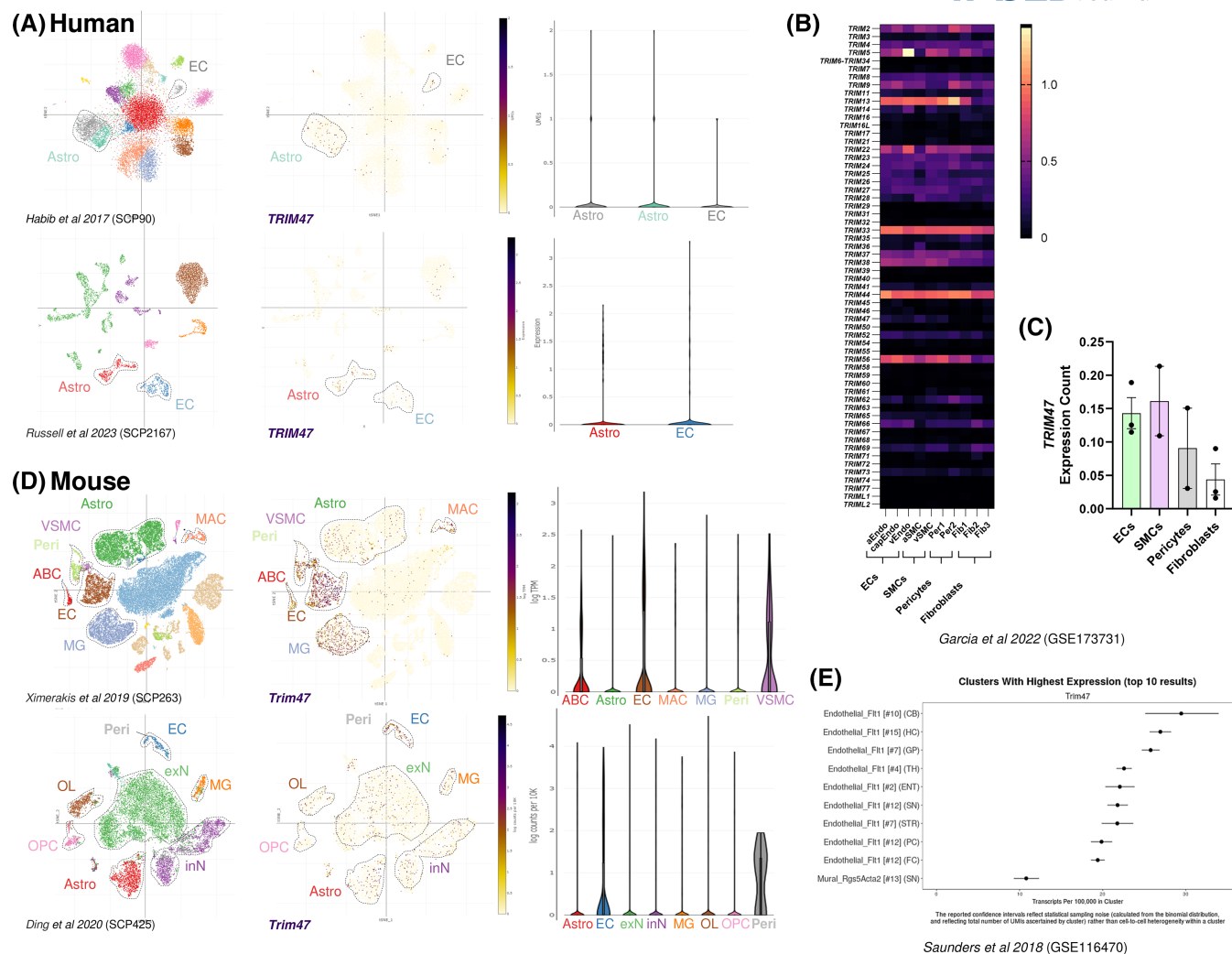To test if the association between *TRIM47* and autophagy is conserved in the mouse model, we investigated

FIGURE 1 *TRIM47* expression is enriched in brain ECs in human and mouse. (A) Single-cell portal-based scRNAseq exploration with t-SNE (t-distributed stochastic neighbor embedding) visualization of gene expression in human brain tissue (accession: SCP90 and SCP2167). *Left*, t-SNE representation of all detected brain cell types *Right*, t-SNE representation of human *TRIM47* expression enriched in the brain endothelial cells and astrocytes. All cell labels are color coded to the tSNE map. The expression level of each cell type is shown on the volin plot. (B) Exploration of *TRIM* family transcription in a scRNAseq library of healthy human cerebrovascular cells (GSE173731), with *TRIM47* expression shown on (C). (D) Single-cell portal-based scRNAseq exploration with t-SNE visualization of gene expression in mouse (wild-type) brain tissues (accession: SCP263 and SCP425). *Left*, t-SNE representation of all detected brain cell types *Right*, t-SNE representation of mouse *Trim47*expression enriched in the Flt1⁺ endothelial cells. The expression level of each cell type is shown on the volin plot. (E) Exploration of a third scRNAseq of a mouse (wild-type) brain across nine regions showing brain ECs have the highest *Trim47* expression in all regions. ABC, arachnoid barrier cell; aEndo, arterioles endothelial cells; and CB, cerebellum; aSMC, arterioles smooth muscle cell; Astro, astrocytes; capEndo, capillary endothelial cells; EC, endothelial cells; ENT, entopeduncular; exN excitatory neurons; FC, frontal cortex; Fib1/Fib2/Fib3, fibroblasts; GP, globus pallidus; HC, hippocampus; inN, inhibitory neurons; MAC, macrophages; MG, microglia; OL, oligodendrocytes; OPC, OL progenitor cells; PC, posterior cortex; Peri or Per1/Per2, Pericytes; SN, substantia nigra; STR, striatum; TH, thalamus; vEndo, venule endothelial cells; VSMC, vascular smooth muscle cells; vSMC, venule smooth muscle cell.

Trim47 expression in a pulmonary hypertension model (PAH).[67] The PAH model was induced by chemical injection and hypoxia to create an increased right ventricular systolic pressure and right ventricular hypertrophy in the animal subject. This is known to cause pulmonary hypertension and the injury of the endothelium of the lung[67]—a similar situation during hypertension-mediated WMH formation. The lung ECs in the PAH model were

sorted by flow cytometry, and we identified significant enrichment of the autophagic process in the hypertensive condition, as in humans (Figure 3C and Table S3). Among the 49 detectable *Trim* family members, three were significantly downregulated in the ECs and *Trim47* ranked number one (Log$_2$ fold change$=-1.85$, RNA-seq, GSE180169). As the reduction of blood flow during hypertension may cause low laminar shear stress at endothelium and
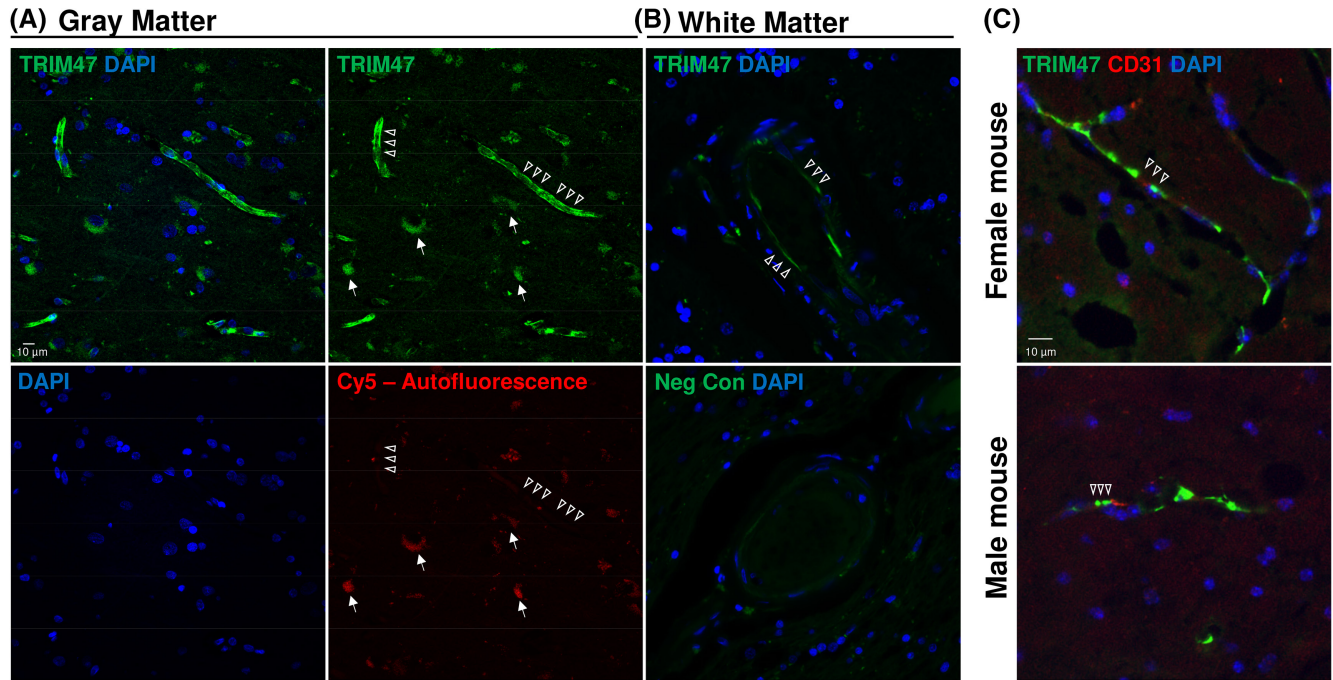
FIGURE 2 Immunohistochemistry of TRIM47 expression human and mouse brain. Representative *TRIM47* (green) immunohistochemistry image of the healthy human frontal cortex of (A) gray matter and (B) white matter, showing the specific expression on endothelial cells. Arrowheads, TRIM47$^+$ endothelial cells; Arrows, autofluorescence from the neuronal cell body (as indicated in the unstained Cy5 signal filter). Negative control with primary antibody omitted is shown on the bottom of (B). (C) Representative immunohistochemistry image of the wild-type mouse corpus callosum with the specific Trim47 expression (green) on CD31$^+$ endothelial cells (red). No difference was found between male and female animals.
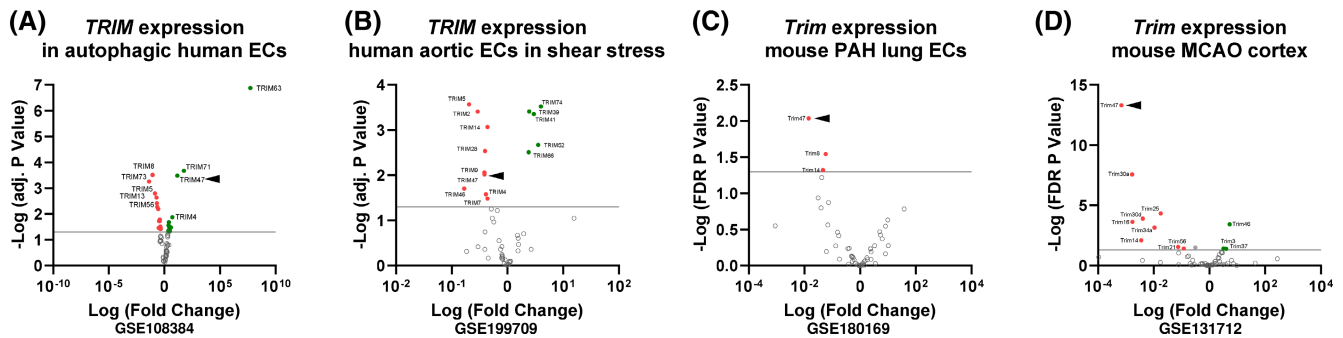
FIGURE 3 TRIM family transcription across hypertensive and cardiovascular disorder models in human and mouse. (A) *TRIM47* expression was significantly regulated in primary HUVEC cells upon overexpression of master autophagy transcription factor TFEB. (B) *TRIM47* expression was downregulated in primary human aortic ECs upon laminar shear stress stimulation, but the level returned to normal after 24 h of recovery. (C) A significant downregulation of *Trim47* expression was found in mouse lung endothelial cells after 3 weeks of pulmonary arterial hypertension modeling. (D) A significant downregulation of *Trim47* expression was found in mouse middle cerebral artery occlusion modeling 24 h upon injury, but the level returned to normal after 28 days of recovery. Extended data are presented see Tables S2 and S3.

reduced autophagy in brain EC of the cerebrovasculature,[25,26] we inquired if *Trim47* expression is altered in an ischemic brain injury model. In a mouse model of transient middle cerebral artery occlusion (MCAO, C57BL/6J, 8–10 weeks of age, occlusion for 1 h),[68] 14 out of the 59 detectable *Trim* family members were significantly and differentially expressed in the ipsilateral cerebral cortex

24 h post-injury, where *Trim47* was the most significantly downregulated member (Log$_2$ fold change = −3.163, RNA-seq, GSE131712). Intriguingly, such downregulation was abolished after 28 days of recovery in the ipsilateral cortex. In a similar mouse MCAO model (Figure 3D, 129S6/SvEv, 8–10 weeks of age, occlusion for 30 min),[69] the brain ECs isolated from the injured brain after 72 h of

recovery similarly showed no changes in any *Trim* family members and no autophagic process was significantly enriched among the differentially expressed genes (FDR-based, RNA-seq, GSE122345, Tables S2 and S3). Details of all the cell types in each study are listed in Tables S2 and S3. Together, these independent datasets suggested the TRIM47 transcription in ECs is significantly upregulated when autophagy is artificially induced, but significantly downregulated when pathophysiology-related (e.g. hypertension- or cerebrovascular dysfunction) autophagy begins.

The bioinformatic inquiry above suggested that TRIM47 belongs to the group of TRIM family members not only involved in ubiquitination-mediated degradation but also in autophagy. Indeed, many of TRIM members interact with human ATG8 (LC3), p62/SQSTM1, and/or ULK1/Beclin1 (TRIM −1, −5, −6, −13, −16, −17, −20, −21, −22, −28, −33, −40, −41, −45, −49, −50, −55, −61, −63, and −76)[36,37] and forms a TRIM-containing complex during autophagosome formation. Nevertheless, TRIM47 was not detected as one of these autophagic regulating members. To clarify, we performed a systemic screening of human and mouse TRIM protein sequences for the LIR motifs using the iLIR database (Table 1).[43,44] LIR motif is the consensus amino acid sequence responsible for autophagic functions. This consensus sequence includes WxxL and xLIR, where **W**xx**L** is the canonical consensus sequence of the LC3B interacting site where x can be any amino acid. The consensus was then extended as xLIR, where the six amino acid residues can be any combination of (ADEFGLPRSK)(DEGMSTV)(**WFY**)(DEILQTV)(ADEFHIKLMPSTV)(**ILV**). Such motif would also have a higher probability to bind to LC3 if it is located within an anchor, a disordered region with a high potential to be stabilized upon binding.[44] Using the position-specific scoring matrix (PSSM) as the measurement, we found that human TRIM47 attained a PSSM score of 14 and it is within the threshold range of the verified xLIR molecules (PSSM = 13–17).[44] Importantly, the xLIR (NQWEQL) motif in human TRIM47 fits within an anchor region. Such a potential LC3 interacting site was conserved in mouse Trim47 (SQWEQL). Although this motif is not embedded within an anchor, the xLIR in Trim47 attained a PSSM score of 16 and within the threshold of verified xLIR-containing proteins. Importantly, a low PSSM score was found in human TRIM65 (9) and mouse Trim65 (8), the other TRIM family member identified in the 17q25 locus, and therefore we focus on TRIM47 function in autophagy in this study.

To demonstrate the putative autophagic function of TRIM47, we performed a structural analysis of the potential TRIM47-LC3B interactions in silico. As no prior X-ray crystallography-based or NMR-based study is available, we first predicted the protein folding structure of human TRIM47 using the Phyre2 Protein Fold Recognition Server.[45] Under the intensive mode of simulation, the final TRIM47 model mapped on the templates of TRIM20 (PDB: 4CG4; Sequence identity 16%, Confidence 100%), TRIM25 (PDB: 6FLN; Sequence identity 24%, Confidence 100%), and TRIM28 (PDB: 6QAJ; Sequence identity 19%, Confidence 100%), see Figure 4A–C. This model was docked with human LC3B protein in ClusPro server,[47] and we identified the potential interactions between the TRIM47 xLIR motif (N379 and Q380 of NQWEQL) and LC3B (K55 and R14, PDB: 3VTU) with a distance of 2.7–2.9 Å (Table S4). To validate this interaction, we repeated the LC3B docking experiment with a new artificial intelligence-based human TRIM47 model predicted by Alphafold[46] (Alphafold: Q96LD4. Figure 4D–F). In this docking experiment, we similarly identified potential interactions between the TRIM47 xLIR motif and LC3B, but through different residues, where the W381, Q383, and L384 of NQWEQL bound to I21, R72, and V93 of LC3B (PDB: 3VTU) with a distance between 2.3 and 4.1 Å. Importantly, the putative NQWEQL interacting contacts at R14 and R72 are identical to the known LC3B binding site at hydrophobic pockets 1 and 2 (HP1 near helix α1 and HP2 near helix α3; equivalent to residue R10 and R69 of PDB: 5WRD, respectively).[70] Furthermore, the K55 contact site is also a known basic residue and electrostatic binding site important for p62/SQSTM1-LC3 interactions (equivalent to residue K50).[71] To test if Trim47-LC3B interaction is conserved in mouse, we docked mouse Trim47 (Alphafold: Q8C0E3) and mouse LC3B (Alphafold: Q9CQV6) and identified a similar binding as in human (Figure 4G–I). Although the binding residues between the mouse xLIR in Trim47 (SQWEQL) and LC3 at F80 and M88 were not known sites of interaction important for autophagy, the potential interaction (Energy weighted score) is comparable to that in human (See Table S4). Together, this docking simulation shows that TRIM47 interacts with LC3B in human and mouse.

The bioinformatic and in silico analysis thus far suggested that TRIM47 is highly expressed by ECs in the brain and is a plausible partner of LC3B during autophagic conditions. The response of *TRIM47* expression in different conditions (see Figure 3) also suggested that TRIM47 is one of the negative regulators of autophagy in the TRIM family.[37] We experimentally tested these findings on a murine brain-derived endothelial cell line, bEnd.3, using a pharmacological approach. By applying 3-methyladenine (3-MA; 0, 0.1, 1 mM) and rapamycin (Rapa, 0, 20 and 200 nM) in full medium for 24 h, we modulated autophagy inhibition and activation on bEnd.3, respectively.[72,73] At the transcription level, 3-MA and Rapa induced differential expression of autophagy genes at the

TABLE 1 Screening of LIR (LC3-interacting region)-motif among known autophagy-associated TRIM family members in human and mouse.

Human

Gene symbol	NCBI protein accession	Motif	Start	End	Pattern	PSSM score	LIR in anchor
SQSTM1	NP_003891.1	xLIR	336	341	DDWTHL	24	Yes
TRIM47	NP_258411.2	WxxL	379	384	NQWEQL	14	Yes
TRIM28	AAH04978.1	WxxL	515	520	EDYNLI	13	Yes
TRIM63	NP_115977.2	WxxL	305	310	MDFFTL	10	Yes
TRIM41	NP_291027.3	WxxL	315	320	SEFGRL	7	Yes
TRIM20	NP_000234.1	xLIR	523	528	SEWELL	20	No
TRIM13	NP_998755.1	WxxL	284	289	SQWEDI	17	No
TRIM21	NP_003132.2	WxxL	9	14	MMWEEV	16	No
TRIM25	NP_005073.2	xLIR	303	308	DEFEFL	16	No
TRIM49	NP_065091.1	WxxL	41	46	LNWQDI	15	No
TRIM5	NP_001397887.1	WxxL	183	188	ADFEQL	14	No
TRIM6	NP_001003818.1	WxxL	326	331	SYWVDV	14	No
TRIM50	NP_835226.2	xLIR	177	182	REFQEL	13	No
TRIM22	NP_006065.2	WxxL	173	178	KNYIQI	9	No
TRIM55	NP_908973.1	WxxL	213	218	EKFDYL	9	No
TRIM65	NP_775818.2	xLIR	333	338	LTFDPV	9	No
TRIM17	NP_001020111.1	WxxL	401	406	STFSAL	9	No
TRIM40	NP_001273562.1	WxxL	238	243	VIYPQL	0	No

Mouse

Gene symbol	NCBI protein accession	Motif	Start	End	Pattern	PSSM score	LIR in anchor
Sqstm1	NP_035148.1	xLIR	338	343	DDWTHL	24	Yes
Trim28	EDL38082.1	WxxL	515	520	EDYNLI	13	Yes
Trim63	NP_001034137.2	WxxL	305	310	MDYFTL	11	Yes
Trim20	XP_006522424.1	WxxL	227	232	EVYVYL	8	Yes
Trim41	NP_663352.2	WxxL	315	320	SEFGRL	7	Yes
Trim21	NP_001076021.1	xLIR	5	10	KMWEEV	18	No
Trim47	NP_001192010.1	WxxL	383	388	SQWEQL	16	No
Trim25	NP_033572.2	xLIR	302	307	DEFEFL	16	No
Trim6	NP_001013637.1	WxxL	298	303	SYWVDV	14	No
Trim5	NP_001297531.1	WxxL	296	301	RYWVQV	13	No
Trim50	NP_839971.1	xLIR	177	182	REFQEL	13	No
Trim13	NP_001157692.1	WxxL	284	289	SQWGDI	12	No
Trim17	NP_112449.1	xLIR	187	192	EEFQKV	11	No
Trim55	NP_001074750.1	WxxL	213	218	EKFDHL	10	No
Trm65	NP_848917.2	WxxL	344	349	NQYLHL	8	No
Trim40	NP_001028407.1	WxxL	170	175	LPWHWL	7	No

Note: LIR = WxxL or xLIR; **W**xx**L**, LIR consensus sequence where x can be any amino acid among the four residues; xLIR, LIR consensus sequence where the six residues can be any amino acids as follows (ADEFGLPRSK)(DEGMSTV)(**WFY**)(DEILQTV)(ADEFHIKLMPSTV)(**ILV**). SQSTM encodes Sequestosome 1(or p62) which is a verified LC3 interacting substrate and serves as the positive control.

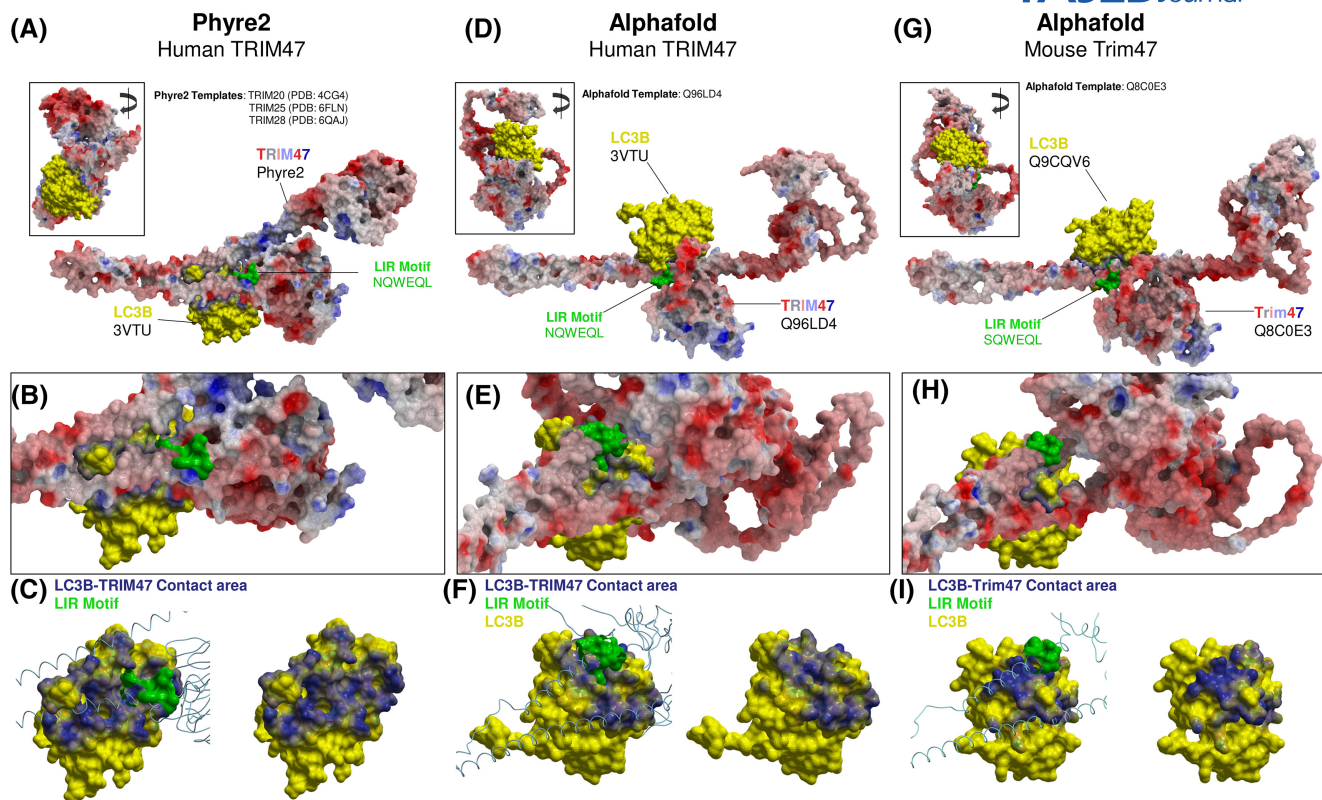Abbreviation: PSSM, position-specific scoring matrix score.

FIGURE 4 Simulation of xLIR motif-LCB interactions in TRIM47 in silico. (A) Phyre2 generated 3D model of TRIM47 (red–gray–blue on electrostatic charge cartoon mesh; model based on PDB: 4CG4, 6FLN, and 6QAJ) docked with human LC3B (yellow; PDB: 3VTU) using ClusPro server.[47] The xLIR sequence NQWEQL is highlighted in green. Right 90° rotation in the inset. (B) Magnified view of the interaction site between xLIR and LC3B. (C) xLIR-LC3B interactions with (*left*) or without (*right*) the ribbon of xLIR (green), where the xLIR-LC3B contact area is highlighted in blue. (D) Human TRIM47 generated by artificial intelligence (red–gray–blue on electrostatic charge cartoon mesh; Alphafold: Q96LD4) docked with human LC3B (Yellow; PDB: 3VTU). The xLIR sequence NQWEQL is highlighted in green. Right 90° rotation in inset (E) Magnified view of the interaction site between xLIR and LC3B. (F) xLIR-LC3B interactions with (*left*) or without (*right*) the ribbon of xLIR (green), where the xLIR-LC3B contact area is highlighted in blue. (G) Alphafold-based Mouse Trim47 (red–gray–blue on electrostatic charge cartoon mesh; Alphafold: Q9CQV6) docked with mouse LC3B (Yellow; Alphafold: Q8C0E3). The xLIR sequence SQWEQL is highlighted in green. Right 90° rotation in inset (H) Magnified view of the interaction site between xLIR and LC3B. (I) xLIR-LC3B interactions with (*left*) or without (*right*) the ribbon of xLIR (green), where the xLIR-LC3B contact area is highlighted in blue.

low concentration, such as *Ulk1*, *Ulk2*, *Map1c3b* (LC3B), *Sqstm1* (p62), and *Gabarap* (Figure 5A,B). At low concentrations, Rapa and 3-MA had no significant effects on gene expression levels, but the pleiotropic effects of 3-MA at different concentrations were observed as reported.[72] Immunoblotting showed that Rapa (200 nM) induced a significant increase in LC3B II/LC3B I conversion indicative of autophagy (Figure 5C).

To visualize the Trim47 expression in association with different stages of autophagy, the treated cells were examined for LC3B colocalization with p-ULK1^{Ser555}, p-p62^{Ser349}, GABARAP, and Trim47, respectively (Figure 5D–H). LC3B is the ATG8 family member that serves as the marker of the autophagy process. The phosphorylation of ULK at serine 555 is mediated by AMPK and is critical for starvation-induced autophagy at the initiation stage.[74] The phosphorylation of p62/SQSTM1 at serine 349 is induced selective autophagy.[75] GABARAP

is an ATG8 family member that is known to associate with LC3B which regulates ULK1 activity in autophagosome formation in response to starvation.[76] The inhibition and promotion of autophagy by 3-MA and Rapa did not alter the overall percentage of LC3B$^+$ bEnd.3 cells, but quantifications showed that the two compounds mediated opposing effects on cytoplasmic LC3B puncta count per field ($p < .05$, Figure 5D). Further quantifications of p-ULK1$^{Ser555+}$ cells showed the percentage of bEnd.3 at the initiation stage was significantly reduced by 3-MA (by 10.1%, 0.1 mM, $p < .05$) but increased by Rapa (by 14%, 20 nM, $p < .01$, Figure 5I). A 2.3-fold difference in LC3B-p-ULK1^{Ser555} double-positive cells was found between 3-MA and Rapa treatment, suggesting differential levels of autophagy induction, as expected (Figure 5J). In these conditions, the number of p-p62^{Ser349} positive and LC3B-p-p62^{Ser349} double positive bEnd.3 cells remained unchanged, suggestive of minimal selective autophagy.
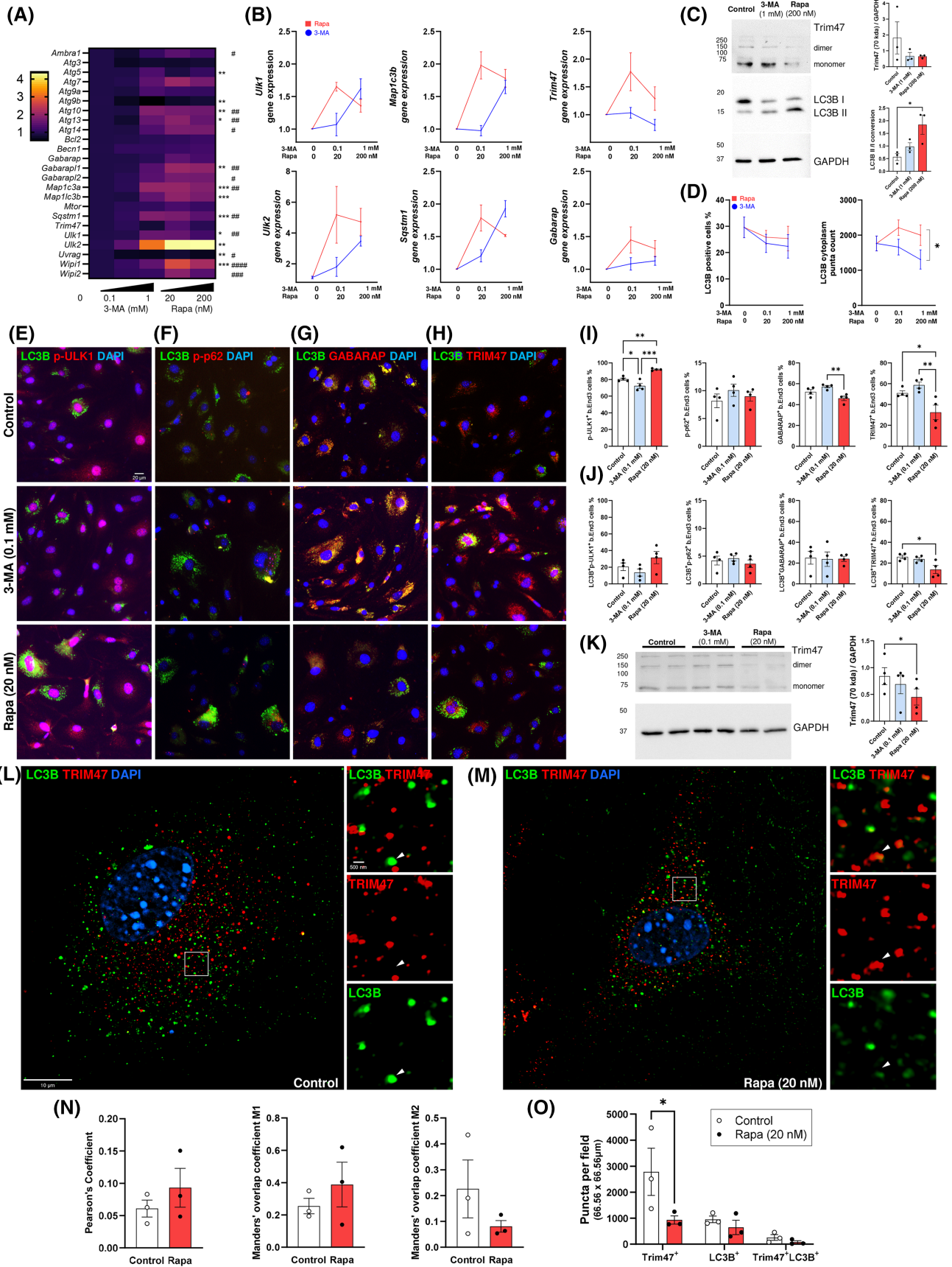
FIGURE 5 Trim47 expression is modulated by rapamycin-mediated autophagy induction in brain endothelial cells. (A) Heatmap of gene expression across autophagy-related genes in bEnd.3 cells upon autophagy inhibition by 3-MA (0.1 and 1 mM) and induction by Rapa (20 and 200 nM). The statistical significance of gene expression changes mediated by 3-MA and Rapa were denoted by * and #, respectively. (B) The concentration-dependent effects of 3-MA and Rapa were exemplified by *Ulk1*, *Ulk2*, *Map1c3b*, *Sqstm1/p62*, *Trim47*, and *Gabarap* induced by 3-MA and Rapa. Of note, the high concentration of 3-MA mediated autophagy in the full medium as reported earlier.[72] (C) Immunoblot showing Trim47 expression at both the monomer (70 kDa) and dimer (~140 kDa) form were reduced by autophagy induction at high concentration of 3-MA (1 mM) and Rapa (200 nM) indicated by the significant LC3B conversion. (D–G) Representative immunocytochemistry image showing the colocalization between LC3B with p-ULK1^{Ser555}, p-p62^{Ser349} GABARAP, and Trim47, respectively. (H) Quantification of the LC3B$^+$ cells and LC3B$^+$ puncta in bEnd.3 cells showed a significant difference between 3-MA and Rapa treatment. (I) Quantification of p-ULK1^{Ser555}, p-p62^{Ser349} GABARAP, and Trim47-expressing cells upon 3-MA and Rapa treatment. (J) Quantification of colocalization between LC3B with p-ULK1^{Ser555}, p-p62^{Ser349} GABARAP, or Trim47 showed a significant reduction of Trim47-LC3B double-positive cells upon Rapa treatment. (K) Immunoblot shows the reduction of Trim47 monomer (70 kDa) by a low concentration of Rapa (20 nM), but not 3-MA (0.1 mM), as in the immunocytochemistry. One-way ANOVA repeated measures followed by Tukey's multiple comparisons test (* or #$p < .05$; ** or ##$p < .01$, *** or ###$p < .001$ and ####$p < .0001$). (L) Structured Illumination Microscopy (SIM)-based super-resolution image of the LC3B and Trim47 at close proximity under control conditions, in which the inset area is shown at a higher magnification on the right. (M) SIM-based super-resolution image of the LC3B and Trim47 at close proximity after Rapa treatment (20 nM, 24 h), in which the inset area is magnified on the right. Scale bar = 10 μm and 500 nm, respectively. (N) Pearson coefficients and Mander's coefficients of the colocalization between TRIM47 and LC3B signal derived from the JACoP analysis in ImageJ ($p > .05$, unpaired *t*-test, $n = 3$).[55–57] (O) Quantification of SIM-detected puncta showed that Rapa (20 nM) exerts an overall effect on puncta number ($p = .0338$, $n = 3$). Two-way ANOVA repeated measures followed by Šídák's multiple comparisons test.

The bEnd.3 cells expressing GABARAP, an ATG8 family member that mediates opposing function against LC3,[76] was significantly lowered by Rapa compared with 3-MA (20%, $p < .01$). Finally, immunocytochemistry showed that Trim47 expression appeared as puncta and was localized both in the cytoplasm and nucleus (Figure 4H). While autophagy inhibition by 3-MA increased Trim47$^+$ bEnd.3 cells by 15.3% (vs. control), autophagy activation by Rapa reduced Trim47$^+$ bEnd.3 cells by 36.1% (vs. control, $p < .05$) (Figure 5I). Of note, the significant difference in Trim47$^+$ bEnd.3 cell numbers between 3-MA and Rapa treatments appeared as an opposing trend to p-ULK1^{Ser555} induction. The reduction of Trim47 monomer (70 kDa) by low concentration of Rapa (20 nM), but not 3-MA (0.1 mM), showed in the immunocytochemistry was confirmed by immunoblotting (Figure 5K).

As the colocalization between Trim47 and LC3B (Figure 5D) was highly comparable to that between GABARAP and LC3B (Figure 5F), and such Trim47$^+$ LC3B$^+$ double positive cells were significantly reduced after Rapa treatment (Figure 5G), these data suggested that Trim47 is closely associated with LC3B as predicted by the in silico model and it may be a negative regulator of autophagy. Indeed, using SIM-based super-resolution microscopy, we observed the close proximity between LC3B and Trim47 puncta in control and Rapa (20 nM) treatment conditions (Figure 5L,M) at a resolution <200 nm. Using the Costes randomization analysis approach, the observed colocalization was significant in the control and Rapa condition ($p < .01$) versus the corresponding image with randomized pixel blocks.[55,56] However, no significant differences in Pearson coefficient, M1 and M2 overlap coefficient were found between the control and Rapa (Figure 5N). The measurement of such colocalization on SIM showed that Rapa (20 nM) treatment accounted for 13.8% of the total variance in puncta number ($p = .0338$), where it significantly reduced Trim47 puncta number ($p = .0194$, pairwise; Figure 5O), in consistent with conventional fluorescent microscopy.

Many TRIM members were experimentally verified to interact with key autophagic adaptors including LC3 (i.e., *TRIM5, −17, −20, −21, −22, −28, −41, −49*, and *−55*) or SQSTM1/p62 (i.e., *TRIM5, −13, −17, −21, −22, −28, −49, −50, −55*, and *−63*) and they form TRIM-containing complex during autophagosome formation,[37] which serve as platform for macroautophagy and selective autophagy.[38] However, no significant TRIM47 interaction was detected in this earlier screening assay.[36,37] To examine such potential interactions in the autophagic b.End3 cells, we examined their puncta colocalization between LC3B with known autophagic adaptors including p-ULK1 (p-ULK1^{Ser555}) p62 (p-p62^{Ser349}), GABRARAP and Trim47 with or without 3-MA or Rapa treatment (Figure 6). The increased p-ULK1$^+$ cells were associated with an increase of p-ULK1$^+$ cytoplasmic puncta (Figure 6A,B). Although the number of p-p62$^+$ cells remains unchanged, the p-p62 and p-p62-LC3B$^+$ double-positive puncta per cell was significantly increased by Rapa ($p < .05$, Figure 6C,D). For GABARAP, a known ATG8 family member and an LC3B partner, the average number of GABARAP$^+$ and GABARAP$^+$LC3B$^+$ puncta in each positive cell remained unchanged by 3-MA and Rapa treatment (Figure 6E,F). Finally, colocalization between Trim47$^+$ and LC3B$^+$ puncta was identified (Figure 6G,H). Importantly, although the cell number of Trim47$^+$ LC3B$^+$ b.End3 was significantly reduced by Rapa (Figure 4J), and the Trim47$^+$ and Trim47$^+$LC3B$^+$ puncta
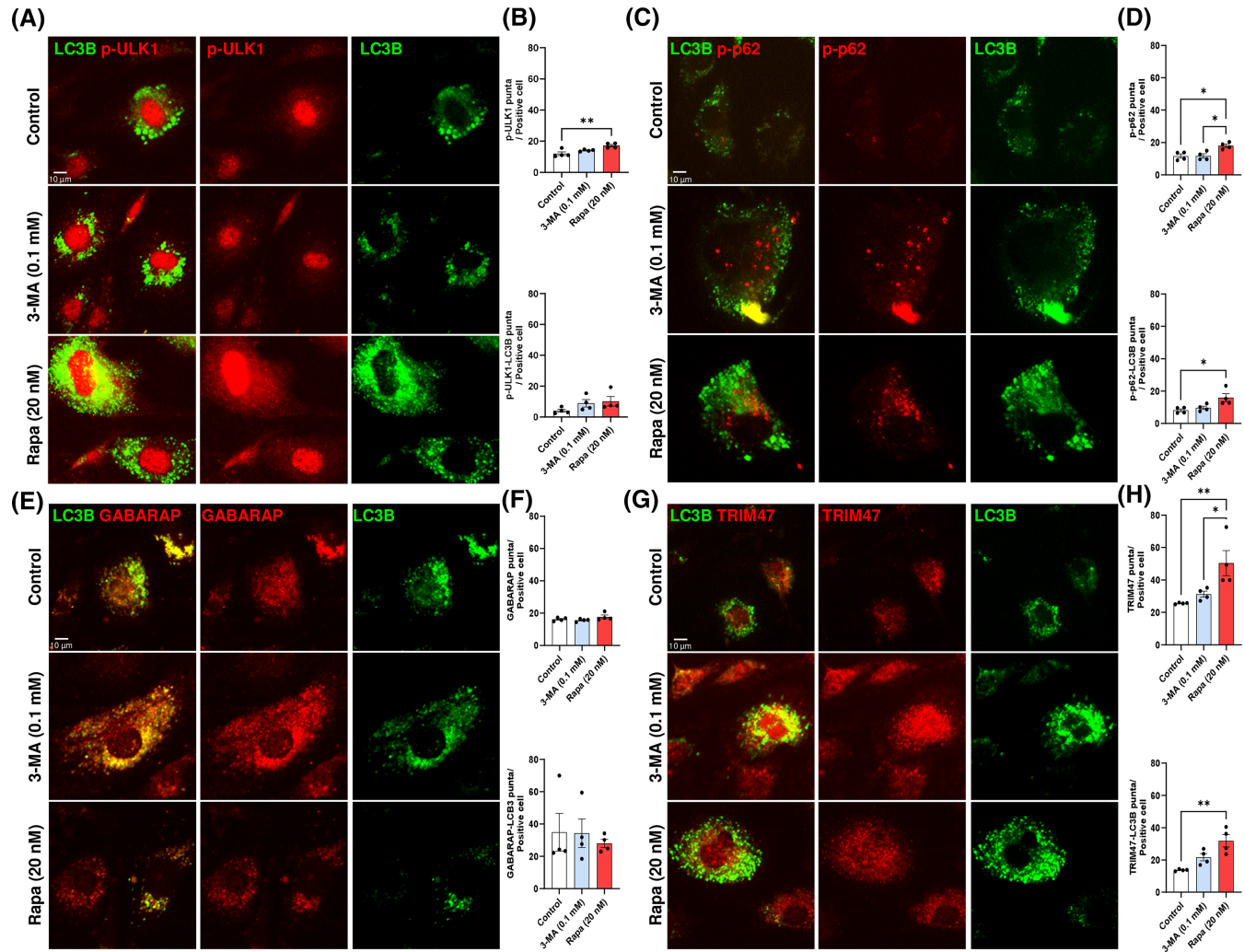
FIGURE 6 Trim47 colocalization with LC3B in autophagic brain endothelial cells. Representative immunocytochemistry image and quantification of (A and B) LC3B-p-ULK1^{Ser555}, (C and D) LC3B-p-p62 (p-p62^{Ser349}), (E and F) LC3B-GABARAP, and (G and H) LC3B-Trim47 colocalization in control, 3-MA, or Rapa treatment. One-way ANOVA repeated measures followed by Tukey's multiple comparisons test (*$p < .05$; **$p < .01$).

in the remaining Trim47-expressing cells were doubled by Rapa treatment (Figure 6H).

The downregulation of *Trim47* in autophagic conditions of ECs and the reduction of Trim47-expressing b.End3 cells upon Rapa treatment suggested that Trim47 may be negatively correlated with autophagy. To investigate if such Trim47 reduction was the outcome of increased autophagic flux, we examined rapamycin-treated b.End3 cells with or without the pre-treatment of Bafilomycin A1 (Baf-A1, 10 nM), a V-ATPase inhibitor that suppresses autophagosome degradation.[77] Autophagic flux inhibition by Baf-A1 significantly prevented Rapa-mediated (20 nM) reduction of Trim47$^+$ b.End3 cells (Figure 7A,B). Indeed, Baf-A1 significantly increased the number of Trim47$^+$ puncta per cell ($p = .001$), the percentage of LC3B$^+$ cells ($p = .0033$) and LC3B$^+$ Trim47$^+$ co-positive cells ($p = .0029$) in all condition, suggesting Rapa-induced Trim47 reduction was mediated through autophagic flux. Gene

expression analysis showed the distinct effects of Rapa and Baf-A1 on key autophagy genes (Figure 7C,D), where Trim47 (*Trim47*) and p62 (*Sqstm1*), were significantly reduced and increased by autophagic flux inhibition by Baf-A1, respectively. Baf-A1 had no effects on LC3B (*Map1lc3b*), Gabarap (*Gabarap*), and Ulk1 (*Ulk1*) at the mRNA level. The results thus far suggested that Trim47 protein expression is significantly reduced with autophagy activation, but such response was abolished when the autophagic flux is impaired. The action and effects of all three pharmacological agents in this study are summarized in Figure 7E.

To test if TRIM47 is a negative regulator of autophagy, we silenced Trim47 (siTrim47) in bEnd.3 cells in the presence or absence of 2DG-mediated starvation. In the gene expression study, siTrim47 induced a significant differential expression of *Atg7*, *Bcl2 Gabarap*, *Gabarapl1*, and *Gabarapl2* (Figure 8A). While 2DG significantly

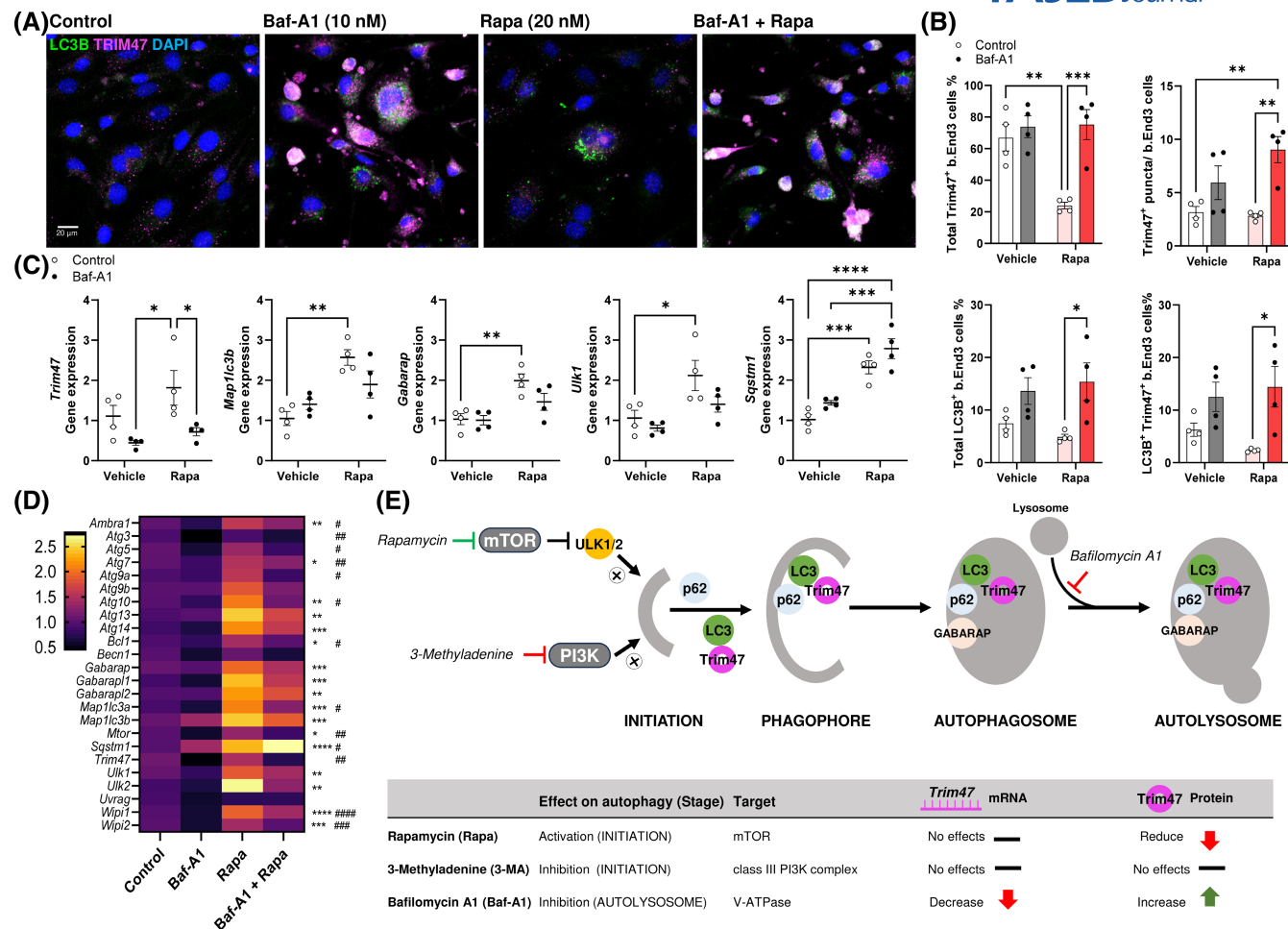**FIGURE 7** Blocking autophagic flux with Bafilomycin A1 increases Trim47 protein (A) Representative immunocytochemistry image and quantification of bEnd.3 cells expressing Trim47 (magenta), and LC3B (green) after Rapamycin (Rapa, 20 nM) with or without Bafilomycin A1 (Baf-A1, 10 nM) pre-treatment. (B) Quantifications of the percentage of b.End3 cells expressing Trim47, expressing LC3B, and co-expressing Trim47 and LC3B, as well as the number of Trim47 puncta per cell (two-way ANOVA followed by Tukey multiple comparisons test, $*p < .05$, $**p < .01$, $***p < .001$). (C) Individual gene expression analysis of *Trim47*, *Map1lc3b*, *Gabarap*, *Ulk1*, and *Sqstm1* demonstrates the differential effect of Rapa and Baf-A1 (D) Heatmap of gene expression analysis of b.End3 cells after Rapamycin (Rapa, 20 nM) with or without Bafilomycin A1 (Baf-A1, 10 nM) pre-treatment. Two-way ANOVA repeated measures followed by Holm–Šídák's multiple comparisons test. The statistical significance of gene expression changes mediated by Rapa and Baf-A1 were denoted by * and #, respectively. (* or #$p < .05$; ** or ##$p < .01$, *** or ###$p < .001$ and **** or ####$p < .0001$) (E) Schematic diagram illustrating the pharmacological agents used in this study on bEnd.3 cells, with Rapamycin activating autophagy pathway through mTOR inhibition, 3-methyladenine inhibiting autophagy through PI3K inhibition and Bafilomycin A1 suppressing autophagic flux via inhibiting lysosomal fusion. The action of these agents and their significant effects on the gene and protein expression of Trim47 in b.End3 cells were summarized in the chart below.

reduced the expression of *Atg7* and *Gabarap*, silencing Trim47 in bEnd.3 cells doubled this expression in all conditions (Figure 8B). *Atg7* is an essential regulator of cytoplasmic to vacuole transport in autophagy while the *Gabarap* family is important for the formation of late autophagosome, and these suggested that the loss of Trim47 may disinhibit autophagy, especially at the later stage. Indeed, in immunocytochemistry, gene silencing of *Trim47* augmented the expression of p-p62[Ser349], p-ULK1[Ser555], and GABARAP in bEnd.3 cells independent of 2DG-mediated starvation (Figure 8C–E). Neither si-Trim47 nor 2DG altered the number of p-ULK+ cells

but siTrim47 significantly increased the number of p-ULK1[Ser555+] in each positive cell ($p = .0097$, Figure 8F). While only 2DG significantly induced p-p62 expressing cells ($p = .0028$) and p-p62 puncta per cell ($p = .0139$), siTrim47 induced the highest number of p-p62 puncta per cell (vs. Control, $p = .0424$, Figure 8G). Silencing Trim47 also significantly increased the percentage of GABARAP-expressing cells ($p = .0009$), but the number of GABARAP puncta was unaffected by either treatment (Figure 8H). The examination of LC3B showed that si-Trim47 significantly increased the number of LC3B+ bEnd.3 cells with or without 2DG treatment (Figure 8I).
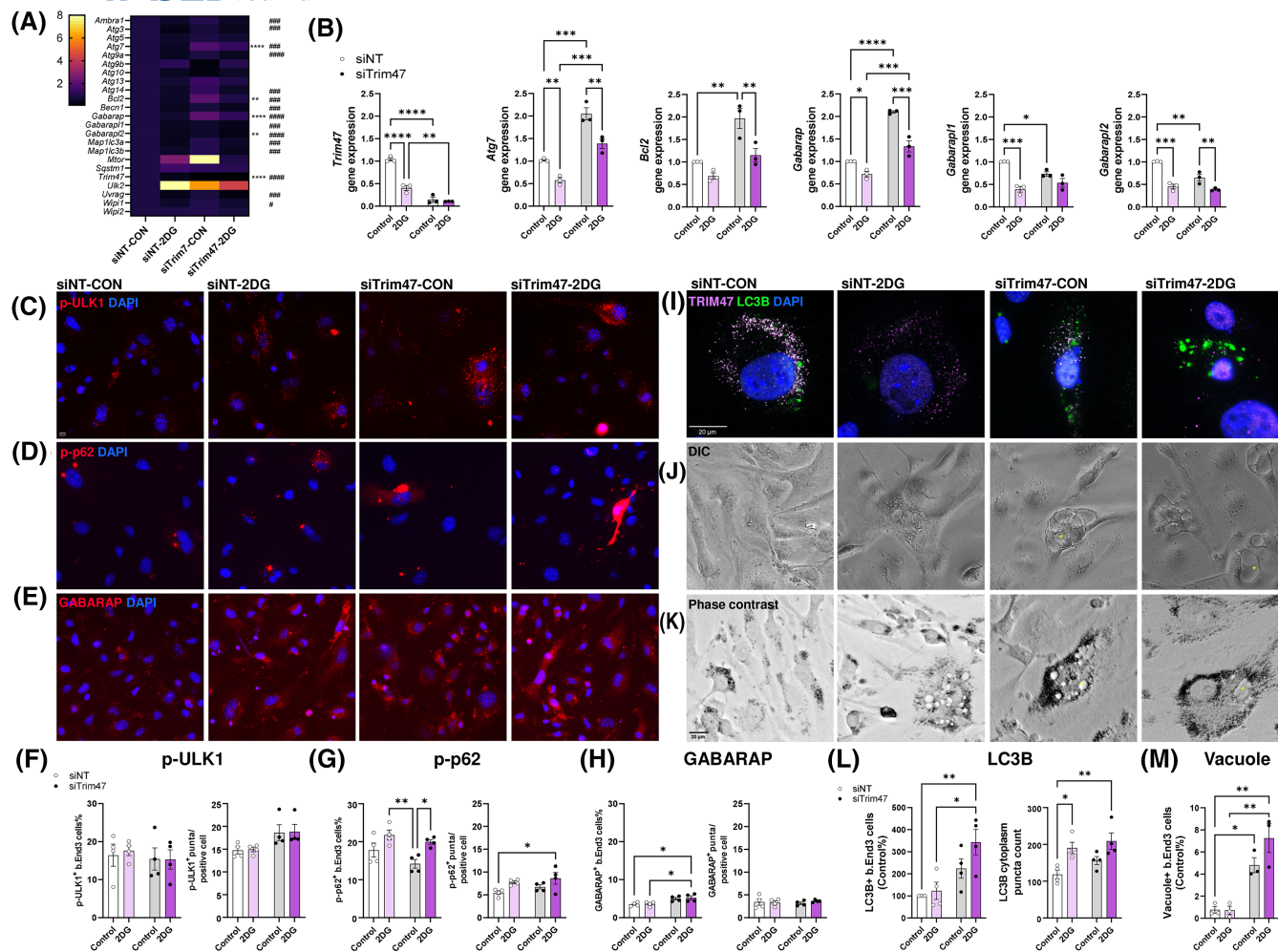
FIGURE 8 Silencing Trim47 increased autophagy in brain endothelial cells. (A) Heatmap of gene expression analysis of b.End3 cells with non-targeted gene silencing (siNT) and siTrim47 with or without 2DG-mediated starvation Two-way ANOVA repeated measures followed by Holm–Šídák's multiple comparisons test ($^{\#}p < .05$, $^{\#\#}p < .01$, $^{\#\#\#}p < .001$, $^{\#\#\#\#}p < .0001$, $^{**}p < .01$, $^{***}p < .001$ and $^{****}p < .0001$). The statistical significance of gene expression changes mediated by siTrim47 and 2DG were denoted by * and $^{\#}$, respectively. (B) Individual gene expression analysis of *Trim47, Atg7, Bcl2, Gabarap, Gabarapl1*, and *Gabarapl2* demonstrates that the loss of *Trim47* disinhibits autophagy. (C–E) Representative immunocytochemistry image of bEnd.3 cells expressing p-ULK1^{Ser555}, p-p62^{Ser349}, and GABARAP treated by siNT or siTrim47 with or without 2DG treatment. (F–H) Quantifications of p-ULK1^{Ser555}, p-p62^{Ser349}, and GABARAP expressing upon siTrim47 with or without 2DG starvation were shown, where (F) silencing Trim47 significantly increased the number of p-ULK1$^{Ser555+}$ puncta in each positive cell ($p = .0097$), (G) induced the highest number of p-p62 puncta per cell (vs. Control, $p = .0424$) and (H) significantly increased the percentage of GABARAP-expressing cells ($p = .0009$). (I) Representative immunocytochemistry image showing the effect of siTrim47 and 2DG on LC3B and Trim47 expression in b.End3 cells. (J and K) Differential interference contrast (DIC) and phase contrast of bEnd.3 cells showing vacuole formation (*) under siTrim47 conditions, respectively. (L and M) Quantification of LC3B$^+$ cells, LC3B$^+$ puncta per cell, and vacuole formation showing that sip-pTrim47 significantly increases autophagy responses in bEnd.3 cells. Two-way ANOVA followed by Tukey multiple comparisons test ($^*p < .05$ and $^{**}p < .01$).

Importantly, the loss of Trim47 also increased the percentage of cells with vacuole formation (Figure 8J,K). Quantifications showed that siTrim47 increased LC3B$^+$ b.End3 cells a 2.2-f and 2.8-fold in control and 2DG treatment, respectively (Figure 8L). Although siTrim47 did not increase the number of LC3B$^+$ puncta, it significantly increased the number of vacuole-positive cells by 4.8-and 7.6-fold in control and 2DG treatment, respectively (Figure 8M). Together, these data indicate that the

loss of Trim47 may disinhibit autophagy in brain ECs and suggest that Trim47 is an endogenous inhibitor of autophagy, possibly at the later stage of the process.

Among the SNPs of *TRIM47* at 17q25 that lead WMH, only one missense variant (rs4600514; NP_258411.2; p.R187W) has potentially damaging consequences.[35] It remains unknown whether this mutation will lead to the loss-of-function or gain-of toxicity-effects on brain ECs. To investigate, we tracked the location of R187 in

the predicted 3D structure of human TRIM47 and mouse Trim47 protein (equivalent to R191) (Figure 9A,B). In both models, the location of this residue is situated in the RING-finger domain which is responsible for E3 ubiquitin ligase function in ubiquitin–proteasome system. However, this residue is far from the LIR motif (NQWEQL or SQWEQL) that is responsible for autophagy function. Yet, TRIM family members are known to form homodimers, heterodimers, and oligomers which may in turn contribute to the recognition of diverse substrates and catalytic regulations.[78,80] We asked if the TRIM47 model may form the anti-parallel coiled-coil dimerization as in TRIM25,[78,81] and whether the residue at R187 may have any implications on the dimerization

(Figure 9C–E). The in silico simulation showed that it is likely that TRIM47 may form coiled-coil dimerization as in TRIM25, but the RING-finger domain remains distant from the dimerization sites (Figure 9C–E). To validate the TRIM47 dimerization, we resolved proteins isolated from bEnd.3 cells treated with 2DG in PAGE without sodium dodecyl sulfate denaturation. A significant increase of potential TRIM47 dimers at approximately 140 kDa (143.4 ± 2.5 kDa) and 130 kDa (134.6 ± 2.3 kDa) were identified. In such non-denaturing conditions, a putative oligomer above 250 kDa was also observed (Figure 9F). Given the size of the Trim47 monomer is 70 kDa, these findings suggested that Trim47 may form a homodimer or heterodimer. In addition, the potential
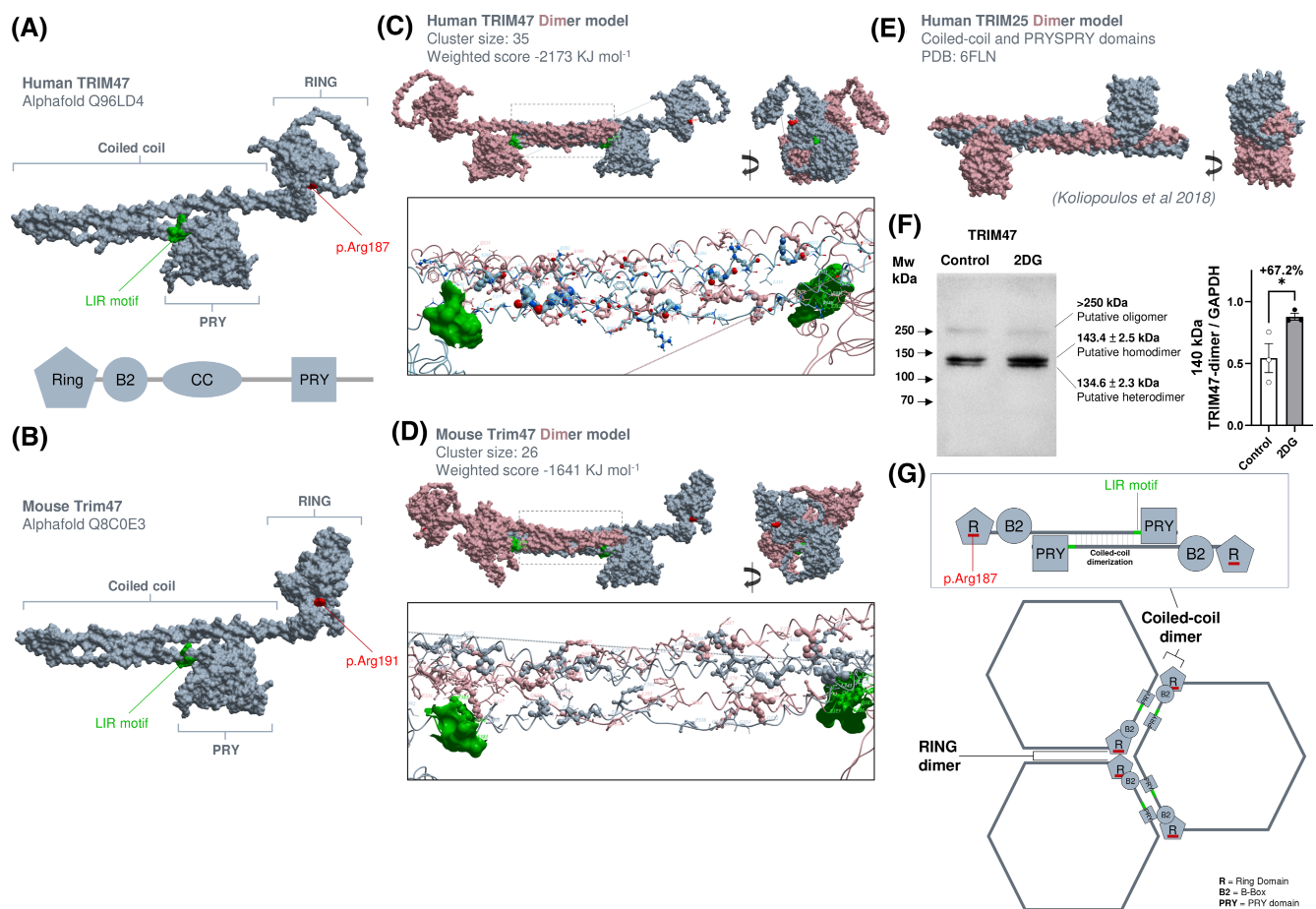
FIGURE 9 WMH associated SNP is located at the RING region of TRIM47 at distance from LIR motif. The in silico model demonstrates (A) human TRIM47 protein and (B) mouse Trim47 structure with the location of the LIR motif in green and the missense variant p.Arg187 (p.Arg191 in mouse) shown in red. (C and D) ClusPro-based simulation of a coiled-coil homodimer of human and mouse TRIM47 model demonstrating the distance between two LIR motifs (green) and the lack of interactions between the missense variant p.Arg187 (red) in the RING domain. (E) Reproduced TRIM25 coiled-coil homodimer model described by Koliopoulos et al.[78] (F) Immunoblotting of bEnd.3 lysate in control and 2DG-treatment resolved under non-denaturing conditions showing the increase of Trim47 dimers at ~140 kDa (143.4 ± 2.5 kDa) and 130 kDa (134.6 ± 2.3 kDa), respectively. The 140 kDa dimer is likely a homodimer of Trim47 (monomer = 70 kDa), while the 130 kDa dimer could be a heterodimer with other Trim family members. An additional band at above 250 kDa suggested that the Trim47 might form oligomers. (G) The formation of TRIM47 coiled-coil homodimers could be the basic building block that may allow the formation of an oligomer as a hexagon mesh of network that may be part of the scaffold (TRIMosome) to facilitate autophagy as earlier described in TRIM5/TRIM5α.[37,79]

formation of coiled-coil dimerization is the basis of the formation of a hexagon mesh network in TRIM5/TRIM5α which bridges the RING domains between two molecules and provides a scaffold as an oligomer for autophagy.[37,82] The dimerization and putative oligomerization of TRIM47 suggested that a similar oligomerization is plausible (Figure 9G).

4 | DISCUSSION

WMH formation is highly correlated with cognitive decline in aging and the progression of age-related dementia. The common identification of genetic risk locus at 17q25 found in GWAS studies has provided clues toward the molecular mechanism of WMH formation.[29,30,33,34] Here, we proposed that *TRIM47*, one of the two TRIM family members at this genetic locus, is highly expressed in the brain ECs and plays a role in autophagy. We identified the potential binding sites with the key autophagy adaptor LC3B in silico and found that TRIM47 is a negative regulator of autophagy in vitro. Autophagy is the key process for ECs remodeling during hypertension flux,[26] and, in turn, hypertension is a major physiological risk factor for WMH formation.[16–18] Our results support that loss of TRIM47 may lead to uncontrolled autophagosome formation, and abnormally increased brain ECs autophagy, which might lead to WMH formation.

The 80 plus members of the TRIM family not only serve as E3 ubiquitin ligases but also play a role in autophagy. In a systemic knockdown screening of 67 human *TRIM* in HeLa cells, it was found that TRIM members can be positive (TRIM3, −5, −6, −22, −23, −28, −31, −34, −38, −41, −42, −44, −45, −48 to −50, −55, −58, −59, −61, −73, and −74) or negative (TRIM1, −2, −10, −17, −26, −33, −51, −65, −72, and −76) regulators of autophagy at different stages.[37,83] In this important study, TRIM47 did not research statistical significance in their screening assay and was missed in their downstream study.[37] Our hypothesis that TRIM47 dysfunction may lead to EC pathology during WMH formation is supported by a recent study showing that the TRIM47 knockdown resulted in an increase of EC permeability in vitro.[35] The authors utilized a simple transwell model and showed that the permeability of two independent human brain EC cell lines was increased after siTRIM47 treatment. Nevertheless, this study did not address the cellular mechanism connecting the TRIM47 loss-of-function and permeability change. The two key cellular homeostasis processes important for EC functions, ubiquitination, and autophagy,[66,84] are both regulated by TRIMs. TRIM47 was shown to regulate TNFα-mediated lung EC activation by degrading TRAF2 through K63 ubiquitination,[85] but its role in autophagy is unknown. Here, we showed that TRIM47 is highly expressed in the ECs of human and mouse brains, and we demonstrated that *TRIM47* is downregulated among the relevant models of hypertension in EC with ongoing autophagy. Of note, we observed that *Trim47* transcription shifts occur acutely (days) upon experimental ischemic models (see Table S3) and return to normal in chronic models (weeks). Indeed, in our recent report, we detected minimal *Trim47* transcription change in the mouse corpus callosum after a 4-weeks bilateral carotid artery stenosis model simulating subcortical ischemic vascular dementia.[86] These observations suggest that TRIM47 may regulate autophagy at the early stage of cerebral ischemia. TRIM family members regulate autophagy at different stages by targeting adaptor proteins such as AMPK, ULK1, or Beclin1, it is also proposed that these proteins form a TRIM-containing complex during autophagosome formation.[83] As in TRIM5α, a positive regulator of autophagy,[37] we identified the LIR motif (NEWEQL) in TRIM47 and its potential binding partner residues in LC3B using in silico and such interaction was visualized by the super-resolution microscopy.

The putative interaction with LC3B may confer the autophagy regulatory function to TRIM47. In bEnd.3 cells, autophagy inhibition mediated by 3-MA and autophagy activation mediated by rapamycin were associated with Trim47 upregulation and downregulation, respectively. This opposing expression pattern suggested that Trim47 may regulate autophagy in EC. The gene silencing experiment supported that Trim47 is a negative regulator of autophagy in brain ECs. Other TRIM family members negatively regulate autophagy by targeting different key autophagic factors such as TFEB,[87] AMPK,[88] or Beclin1[89] through proteasome degradation, transcription, or microRNA regulations.[83] These regulatory functions of TRIM protein are highly associated with their intracellular distribution, for instance, TRIM52 regulates immune functions by acting in the nucleus[90] while TRIM20 regulates E3 ligase functions in the cytoplasm.[36] The dual localization of Trim47 suggested that it may serve autophagy regulatory functions in the nucleus and cytoplasm of brain ECs. Silencing Trim47 not only resulted in a significant upregulation of players (*Atg7 Bcl2* and *Gabarap*) important for autophagosome formation[79,91] but also increased the ECs with phosphorylation of ULK1 and p62 as well as vacuole formation. As ULK-mediates the phosphorylation of p62,[92] Trim47 is therefore pivotal to both early and later stages of autophagy.[74] TRIM65, the other TRIM member at locus 17q25, is known to inhibit autophagy also by controlling *Atg7* expression in lung cancer cells.[39] It remains obscure whether the TRIM47 and TRIM65 mediate autophagy regulation by jointly targeting *Atg7* in brain ECs, but it warrants further investigation.

The possible TRIM47 the pathogenic variant (rs4600514, missense, NP_258411.2: p.Arg187Trp) is located in the RING domain and may have a direct implication on the E3 ligase activity. Yet, TRIM members are known to form homodimers, heterodimers, and oligomers to function,[36] which opens up other possible mechanisms by which this particular variant might increase the risk of WMH. First, the self-association of two TRIM monomers is enabled by the highly conserved coiled coil which forms an interdigitating anti-parallel helical hairpin.[81] Such a homodimer is proposed to be the building block of more complex oligomers with the TRIM5/TRIM5α being the best-studied example. Second, the dimerization between the RING domain is critical for E3 ligase activity and is conserved among TRIM subfamily C-IV where TRIM47 belongs.[93] Finally, as exemplified by TRIM5/TRIM5α, these antiparallel, coiled-coil homodimers with the RING domain at both ends may self-assemble into trimers of heterodimer, and ultimately form a hexagon scaffold (TRIMosome) to facilitate autophagy.[37,82] Our in silico modeling shows that TRIM47 can form such a dimer and our in vitro work shows that a dimeric form of TRIM47 is increased when autophagy is induced. Although the distance (194 amino acids) between the RING domains and LIR motif at the PRY domain would seem to make the missense variant more relevant to ubiquitination than to autophagy, the potential dimerization or oligomerization (e.g., a hexagonal structure, see Figure 9G) of TRIM47 may impact autophagy as well as E3 ligase activity. Such potential spatial re-arrangement may also bring the missense p.Arg187Trp of rs4600514 to close proximity. TRIM family members are most likely to form heterodimers with structurally related members.[81] We note that TRIM47 and TRIM65, both encoded by genes at the 17q25 locus are both members of the same C-IV subfamily.[36] This leads us to speculate that the two proteins may be coordinately regulated during normal physiological functions by forming heterodimers specifically targeted to autophagic functions, and warrants further investigations.

Apart from rs4600514, there are at least three *TRIM47* eQTLs (expression quantitative trait locus) including rs936393, rs9894383, and rs3744017 identified at 17q25.1.[29] Unlike rs4600514, other eQTLs are predicted to play regulatory functions on TRIM47 expression. As we are limited by *Trim47* knockdown in this study, it remains unknown how these variants would implicate TRIM47 expression and/or function. Indeed, the regulation of TRIM47 expression is likely complex, as we have shown that genetic induction (i.e., TFEB overexpression) of autophagy will upregulate *TRIM47*, while physiological or pharmacological stimulation of autophagy (i.e., shear stress or rapamycin) will downregulate *TRIM47*. TRIM47 appears to be part of a negative feedback mechanism to regulate autophagy that prevents abnormal levels of continuous induction. While the focus of the present study is the role of TRIM47 in autophagy, the RING domain in TRIM47 is suggestive of ubiquitin E3 ligase function for the ubiquitin–proteasome system.[36] How TRIM47 is involved in both pathways, and their possible crosstalk, remains an open question. Future studies with patient-derived cells (ECs derived from iPSC) will be necessary for elucidating the pathogenicity of these eQTLs, and the regulatory function of TRIM47 in autophagy and ubiquitination for protein degradation.

The present study provides proof-of-concept evidence demonstrating the regulatory function of Trim47 in EC autophagy, but the scope is limited by the in silico and in vitro experiments. Our experiments suggested a putative interaction between TRIM47 and LC3, their biochemical interactions should be further tested using assays such as co-immunoprecipitation, proximity ligation, or fluorescence energy transfer. To address if impaired Trim47 could result in BBB and WMH formation, future studies should investigate the effect of *Trim47*-knockout mouse models in vivo, the effects of aging, and brain regions on Trim47 expression. Brain vasculature is a highly dynamic system, where flexibility is conferred by the process of autophagy in the ECs that form an important part of its structure. Our findings support a model in which dysfunctional TRIM47 contributes to autophagy failure in brain ECs and in this way compromises the remodeling of the cerebrovasculature, especially in conditions favoring hypertension. The impaired responsiveness to the normal (or enhanced) shear stresses that result confer an elevated risk of WMH development and offers a potential mechanistic explanation for the link between the rs4600514 TRIM47 missense mutation and the increased risk of WMH.

DISCLOSURES

The authors declare no competing financial interests.

DATA AVAILABILITY STATEMENT

The datasets during and/or analyzed during the current study are available from the corresponding author upon reasonable request.

ETHICS APPROVAL AND CONSENT TO PARTICIPATE

This study involves human tissue: All human tissue experiments from the brain bank in the Neuropathology Core of Alzheimer's Disease Research Center (ADRC) at University of Pittsburgh Medical Center with approvals from the Committee for Oversight of Research and Clinical Training Involving Decedents at University of Pittsburgh. The ADRC is funded by NIH P30 AG066468-02. This cohort of postmortem tissue from the brain bank is ruled exempt by IRB at University of Pittsburgh Research as it only involves the collection or study of existing data, documents, records, pathological specimens, or diagnostic specimens, if these sources are publicly available or if the information is recorded by the investigator and in such a manner that subjects cannot be identified, directly or through identifiers linked to the subjects. This study involves animals: All animal experiments in this study are approved by Animal Subjects Ethics Sub-committee (ASESC), Research Committee, The Hong Kong Polytechnic University with ASESC reference number 20-21/167-HTI-R-GRF.

CONSENT FOR PUBLICATION

Not applicable.

ORCID

Sunny Hoi-Sang Yeung https://orcid.org/0000-0002-7362-7133
Ralph Hon-Sun Lee https://orcid.org/0009-0003-0445-881X
Gerald Wai-Yeung Cheng https://orcid.org/0000-0002-1199-3592
Iris Wai-Ting Ma https://orcid.org/0009-0008-1407-0946
Karl Herrup https://orcid.org/0000-0001-7786-5844
Kai-Hei Tse https://orcid.org/0000-0001-7287-3984

REFERENCES

1. Alber J, Alladi S, Bae HJ, et al. White matter hyperintensities in vascular contributions to cognitive impairment and dementia (VCID): knowledge gaps and opportunities. *Alzheimers Dement (N Y)*. 2019;5:107-117. doi:10.1016/j.trci.2019.02.001

2. Roseborough AD, Saad L, Goodman M, Cipriano LE, Hachinski VC, Whitehead SN. White matter hyperintensities and longitudinal cognitive decline in cognitively normal populations and across diagnostic categories: a meta-analysis, systematic review, and recommendations for future study harmonization. *Alzheimers Dement*. 2023;19:194-207. doi:10.1002/alz.12642

3. Au R, Massaro JM, Wolf PA, et al. Association of white matter hyperintensity volume with decreased cognitive functioning: the Framingham heart study. *Arch Neurol*. 2006;63:246-250. doi:10.1001/archneur.63.2.246

4. Brown R, Low A, Markus HS. Rate of, and risk factors for, white matter hyperintensity growth: a systematic review and meta-analysis with implications for clinical trial design. *J Neurol Neurosurg Psychiatry*. 2021;92:1271-1277. doi:10.1136/jnnp-2021-326569

5. Vergoossen LWM, Jansen JFA, van Sloten TT, et al. Interplay of white matter Hyperintensities, cerebral networks, and cognitive function in an adult population: diffusion-tensor imaging in the Maastricht study. *Radiology*. 2021;298:384-392. doi:10.1148/radiol.2021202634

6. Prins ND, Scheltens P. White matter hyperintensities, cognitive impairment and dementia: an update. *Nat Rev Neurol*. 2015;11:157-165. doi:10.1038/nrneurol.2015.10

7. Habes M, Erus G, Toledo JB, et al. White matter hyperintensities and imaging patterns of brain ageing in the general population. *Brain*. 2016;139:1164-1179. doi:10.1093/brain/aww008

8. Fazekas F, Kleinert R, Offenbacher H, et al. Pathologic correlates of incidental MRI white matter signal hyperintensities. *Neurology*. 1993;43:1683-1689.

9. Gouw AA, Seewann A, Vrenken H, et al. Heterogeneity of white matter hyperintensities in Alzheimer's disease: post-mortem quantitative MRI and neuropathology. *Brain*. 2008;131:3286-3298. doi:10.1093/brain/awn265

10. Kalaria RN. Neuropathological diagnosis of vascular cognitive impairment and vascular dementia with implications for Alzheimer's disease. *Acta Neuropathol*. 2016;131:659-685. doi:10.1007/s00401-016-1571-z

11. Shim YS, Yang DW, Roe CM, et al. Pathological correlates of white matter hyperintensities on magnetic resonance imaging. *Dement Geriatr Cogn Disord*. 2015;39:92-104. doi:10.1159/000366411

12. Hainsworth AH, Minett T, Andoh J, et al. Neuropathology of white matter lesions, blood-brain barrier dysfunction, and dementia. *Stroke*. 2017;48:2799-2804. doi:10.1161/STROKEAHA.117.018101

13. Bridges LR, Andoh J, Lawrence AJ, et al. Blood-brain barrier dysfunction and cerebral small vessel disease (arteriosclerosis) in brains of older people. *J Neuropathol Exp Neurol*. 2014;73:1026-1033. doi:10.1097/NEN.0000000000000124

14. Montagne A, Nikolakopoulou AM, Zhao Z, et al. Pericyte degeneration causes white matter dysfunction in the mouse central nervous system. *Nat Med*. 2018;24:326-337. doi:10.1038/nm.4482

15. Tse KH, Herrup K. Re-imagining Alzheimer's disease - the diminishing importance of amyloid and a glimpse of what lies ahead. *J Neurochem*. 2017;143:432-444. doi:10.1111/jnc.14079

16. Verhaaren BF, Vernooij MW, de Boer R, et al. High blood pressure and cerebral white matter lesion progression in the general population. *Hypertension*. 2013;61:1354-1359. doi:10.1161/HYPERTENSIONAHA.111.00430

17. Hajjar I, Quach L, Yang F, et al. Hypertension, white matter hyperintensities, and concurrent impairments in mobility, cognition, and mood: the cardiovascular health study. *Circulation*. 2011;123:858-865. doi:10.1161/CIRCULATIONAHA.110.978114

18. Chesebro AG, Melgarejo JD, Leenderbz R, et al. White matter hyperintensities mediate the association of nocturnal blood pressure with cognition. *Neurology*. 2020;94:e1803-e1810. doi:10.1212/WNL.0000000000009316

19. Maillard P, Seshadri S, Beiser A, et al. Effects of systolic blood pressure on white-matter integrity in young adults in the Framingham heart study: a cross-sectional study. *Lancet Neurol*. 2012;11:1039-1047. doi:10.1016/S1474-4422(12)70241-7

20. Hasan-Olive MM, Hansson HA, Enger R, Nagelhus EA, Eide PK. Blood-brain barrier dysfunction in idiopathic intracranial hypertension. *J Neuropathol Exp Neurol*. 2019;78:808-818. doi:10.1093/jnen/nlz063

21. Kim KA, Shin D, Kim JH, et al. Role of autophagy in endothelial damage and blood-brain barrier disruption in ischemic stroke. *Stroke*. 2018;49:1571-1579. doi:10.1161/STROKEAHA.117.017287

22. Zhao Z, Nelson AR, Betsholtz C, Zlokovic BV. Establishment and dysfunction of the blood-brain barrier. *Cell*. 2015;163:1064-1078. doi:10.1016/j.cell.2015.10.067

23. de Meyer GR, Grootaert MOJ, Michiels CF, Kurdi A, Schrijvers DM, Martinet W. Autophagy in vascular disease. *Circ Res*. 2015;116:468-479. doi:10.1161/CIRCRESAHA.116.303804

24. Nussenzweig SC, Verma S, Finkel T. The role of autophagy in vascular biology. *Circ Res*. 2015;116:480-488. doi:10.1161/CIRCRESAHA.116.303805

25. Pires PW, Dams Ramos CM, Matin N, Dorrance AM. The effects of hypertension on the cerebral circulation. *Am J Physiol Heart Circ Physiol*. 2013;304:H1598-H1614. doi:10.1152/ajpheart.00490.2012

26. Vion AC, Kheloufi M, Hammoutene A, et al. Autophagy is required for endothelial cell alignment and atheroprotection under physiological blood flow. *Proc Natl Acad Sci U S A*. 2017;114:E8675-E8684. doi:10.1073/pnas.1702223114

27. de Montgolfier O, Pinçon A, Pouliot P, et al. High systolic blood pressure induces cerebral microvascular endothelial dysfunction, neurovascular unit damage, and cognitive decline in mice. *Hypertension*. 2019;73:217-228. doi:10.1161/HYPERTENSIONAHA.118.12048

28. Forte M, Bianchi F, Cotugno M, et al. Pharmacological restoration of autophagy reduces hypertension-related stroke occurrence. *Autophagy*. 2020;16:1468-1481. doi:10.1080/15548627.2019.1687215

29. Verhaaren BF, Debette S, Bis JC, et al. Multiethnic genome-wide association study of cerebral white matter hyperintensities on MRI. *Circ Cardiovasc Genet*. 2015;8:398-409. doi:10.1161/CIRCGENETICS.114.000858

30. Traylor M, Tozer DJ, Croall ID, et al. Genetic variation in PLEKHG1 is associated with white matter hyperintensities (n = 11,226). *Neurology*. 2019;92:e749-e757. doi:10.1212/WNL.0000000000006952

31. Sarnowski C, Satizabal CL, DeCarli C, et al. Whole genome sequence analyses of brain imaging measures in the Framingham study. *Neurology*. 2018;90:e188-e196. doi:10.1212/WNL.0000000000004820

32. Sargurupremraj M, Suzuki H, Jian X, et al. Cerebral small vessel disease genomics and its implications across the lifespan. *Nat Commun*. 2020;11:6285. doi:10.1038/s41467-020-19111-2

33. Persyn E, Hanscombe KB, Howson JMM, Lewis CM, Traylor M, Markus HS. Genome-wide association study of MRI markers of cerebral small vessel disease in 42,310 participants. *Nat Commun*. 2020;11:2175. doi:10.1038/s41467-020-15932-3

34. Fornage M, Debette S, Bis JC, et al. Genome-wide association studies of cerebral white matter lesion burden: the CHARGE consortium. *Ann Neurol*. 2011;69:928-939. doi:10.1002/ana.22403

35. Mishra A, Duplaà C, Vojinovic D, et al. Gene-mapping study of extremes of cerebral small vessel disease reveals TRIM47 as a strong candidate. *Brain*. 2022;145:1992-2007. doi:10.1093/brain/awab432

36. Hatakeyama S. TRIM family proteins: roles in autophagy, immunity, and carcinogenesis. *Trends Biochem Sci*. 2017;42:297-311. doi:10.1016/j.tibs.2017.01.002

37. Mandell MA, Jain A, Arko-Mensah J, et al. TRIM proteins regulate autophagy and can target autophagic substrates by direct recognition. *Dev Cell*. 2014;30:394-409. doi:10.1016/j.devcel.2014.06.013

38. Kimura T, Mandell M, Deretic V. Precision autophagy directed by receptor regulators - emerging examples within the TRIM family. *J Cell Sci*. 2016;129:881-891. doi:10.1242/jcs.163758

39. Pan X, Chen Y, Shen Y, Tantai J. Knockdown of TRIM65 inhibits autophagy and cisplatin resistance in A549/DDP cells by regulating miR-138-5p/ATG7. *Cell Death Dis*. 2019;10:429. doi:10.1038/s41419-019-1660-8

40. Barrett T, Wilhite SE, Ledoux P, et al. NCBI GEO: archive for functional genomics data sets—update. *Nucleic Acids Res*. 2013;41:D991-D995. doi:10.1093/nar/gks1193

41. Mahi NA, Najafabadi MF, Pilarczyk M, Kouril M, Medvedovic M. GREIN: an interactive web platform for Re-analyzing GEO RNA-seq data. *Sci Rep*. 2019;9:7580. doi:10.1038/s41598-019-43935-8

42. Mi H, Muruganujan A, Ebert D, Huang X, Thomas PD. PANTHER version 14: more genomes, a new PANTHER

GO-slim and improvements in enrichment analysis tools. *Nucleic Acids Res*. 2019;47:D419-D426. doi:10.1093/nar/gky1038

43. Jacomin AC, Samavedam S, Promponas V, Nezis IP. iLIR database: a web resource for LIR motif-containing proteins in eukaryotes. *Autophagy*. 2016;12:1945-1953. doi:10.1080/15548627.2016.1207016

44. Kalvari I, Tsompanis S, Mulakkal NC, et al. iLIR: a web resource for prediction of Atg8-family interacting proteins. *Autophagy*. 2014;10:913-925. doi:10.4161/auto.28260

45. Kelley LA, Mezulis S, Yates CM, Wass MN, Sternberg MJ. The Phyre2 web portal for protein modeling, prediction and analysis. *Nat Protoc*. 2015;10:845-858. doi:10.1038/nprot.2015.053

46. Jumper J, Evans R, Pritzel A, et al. Highly accurate protein structure prediction with AlphaFold. *Nature*. 2021;596:583-589. doi:10.1038/s41586-021-03819-2

47. Kozakov D, Hall DR, Xia B, et al. The ClusPro web server for protein-protein docking. *Nat Protoc*. 2017;12:255-278. doi:10.1038/nprot.2016.169

48. Abagyan R, Totrov M, Kuznetsov D. ICM—A new method for protein modeling and design: applications to docking and structure prediction from the distorted native conformation. *J Comput Chem*. 1994;15:488-506. doi:10.1002/jcc.540150503

49. Mok KK, Yeung SHS, Cheng GWY, et al. Apolipoprotein E epsilon4 disrupts oligodendrocyte differentiation by interfering with astrocyte-derived lipid transport. *J Neurochem*. 2023;165:55-75. doi:10.1111/jnc.15748

50. Montesano R, Pepper MS, Möhle-Steinlein U, Risau W, Wagner EF, Orci L. Increased proteolytic activity is responsible for the aberrant morphogenetic behavior of endothelial cells expressing the middle T oncogene. *Cell*. 1990;62:435-445. doi:10.1016/0092-8674(90)90009-4

51. Spandidos A, Wang X, Wang H, Seed B. PrimerBank: a resource of human and mouse PCR primer pairs for gene expression detection and quantification. *Nucleic Acids Res*. 2010;38:D792-D799. doi:10.1093/nar/gkp1005

52. Bankhead P, Loughrey MB, Fernández JA, et al. QuPath: open source software for digital pathology image analysis. *Sci Rep*. 2017;7:16878. doi:10.1038/s41598-017-17204-5

53. McQuin C, Goodman A, Chernyshev V, et al. CellProfiler 3.0: next-generation image processing for biology. *PLoS Biol*. 2018;16:e2005970. doi:10.1371/journal.pbio.2005970

54. Klionsky DJ, Abdel-Aziz AK, Abdelfatah S, et al. Guidelines for the use and interpretation of assays for monitoring autophagy (4th edition)(1). *Autophagy*. 2021;17:1-382. doi:10.1080/15548627.2020.1797280

55. Dunn KW, Kamocka MM, McDonald JH. A practical guide to evaluating colocalization in biological microscopy. *Am J Physiol Cell Physiol*. 2011;300:C723-C742. doi:10.1152/ajpcell.00462.2010

56. Bolte S, Cordelieres FP. A guided tour into subcellular colocalization analysis in light microscopy. *J Microsc*. 2006;224:213-232. doi:10.1111/j.1365-2818.2006.01706.x

57. Silva P, Hernández N, Tapia H, et al. Tumor-derived hypoxic small extracellular vesicles promote endothelial cell migration and tube formation via ALS2/Rab5/beta-catenin signaling. *FASEB J*. 2024;38:e23716. doi:10.1096/fj.202400265R

58. Analytical Methods Committee Amctb, N. Using the Grubbs and Cochran tests to identify outliers. *Anal Methods*. 2015;7:7948-7950. doi:10.1039/c5ay90053k

59. Habib N, Avraham-Davidi I, Basu A, et al. Massively parallel single-nucleus RNA-seq with DroNc-seq. *Nat Methods*. 2017;14:955-958. doi:10.1038/nmeth.4407

60. Russell AJC, Weir JA, Nadaf NM, et al. Slide-tags: scalable, single-nucleus barcoding for multi-modal spatial genomics. *bioRxiv*. 2023. doi:10.1101/2023.04.01.535228

61. Garcia FJ, Sun N, Lee H, et al. Single-cell dissection of the human brain vasculature. *Nature*. 2022;603:893-899. doi:10.1038/s41586-022-04521-7

62. Ximerakis M, Lipnick SL, Innes BT, et al. Single-cell transcriptomic profiling of the aging mouse brain. *Nat Neurosci*. 2019;22:1696-1708. doi:10.1038/s41593-019-0491-3

63. Ding J, Adiconis X, Simmons SK, et al. Systematic comparison of single-cell and single-nucleus RNA-sequencing methods. *Nat Biotechnol*. 2020;38:737-746. doi:10.1038/s41587-020-0465-8

64. Saunders A, Macosko EZ, Wysoker A, et al. Molecular diversity and specializations among the cells of the adult mouse brain. *Cell*. 2018;174:1015-1030.e16. doi:10.1016/j.cell.2018.07.028

65. Fan Y, Lu H, Liang W, et al. Endothelial TFEB (transcription factor EB) positively regulates Postischemic angiogenesis. *Circ Res*. 2018;122:945-957. doi:10.1161/CIRCRESAHA.118.312672

66. Meng Q, Pu L, Qi M, et al. Laminar shear stress inhibits inflammation by activating autophagy in human aortic endothelial cells through HMGB1 nuclear translocation. *Commun Biol*. 2022;5:425. doi:10.1038/s42003-022-03392-y

67. Rodor J, Chen SH, Scanlon JP, et al. Single-cell RNA sequencing profiling of mouse endothelial cells in response to pulmonary arterial hypertension. *Cardiovasc Res*. 2022;118:2519-2534. doi:10.1093/cvr/cvab296

68. Wu F, Han B, Wu S, et al. Circular RNA TLK1 aggravates neuronal injury and neurological deficits after ischemic stroke via miR-335-3p/TIPARP. *J Neurosci*. 2019;39:7369-7393. doi:10.1523/JNEUROSCI.0299-19.2019

69. Wegner S, Uhlemann R, Boujon V, et al. Endothelial cell-specific transcriptome reveals signature of chronic stress related to worse outcome after mild transient brain ischemia in mice. *Mol Neurobiol*. 2020;57:1446-1458. doi:10.1007/s12035-019-01822-3

70. Wirth M, Zhang W, Razi M, et al. Molecular determinants regulating selective binding of autophagy adapters and receptors to ATG8 proteins. *Nat Commun*. 2019;10:2055. doi:10.1038/s41467-019-10059-6

71. Johansen T, Lamark T. Selective autophagy mediated by autophagic adapter proteins. *Autophagy*. 2011;7:279-296. doi:10.4161/auto.7.3.14487

72. Wu YT, Tan HL, Shui G, et al. Dual role of 3-methyladenine in modulation of autophagy via different temporal patterns of inhibition on class I and III phosphoinositide 3-kinase. *J Biol Chem*. 2010;285:10850-10861. doi:10.1074/jbc.M109.080796

73. Cheng A, Tse KH, Chow HM, et al. ATM loss disrupts the autophagy-lysosomal pathway. *Autophagy*. 2021;17:1998-2010. doi:10.1080/15548627.2020.1805860

74. Egan DF, Chun MGH, Vamos M, et al. Small molecule inhibition of the autophagy kinase ULK1 and identification of ULK1 substrates. *Mol Cell*. 2015;59:285-297. doi:10.1016/j.molcel.2015.05.031

75. Ichimura Y, Waguri S, Sou YS, et al. Phosphorylation of p62 activates the Keap1-Nrf2 pathway during selective autophagy. *Mol Cell*. 2013;51:618-631. doi:10.1016/j.molcel.2013.08.003

76. Grunwald DS, Otto NM, Park JM, Song D, Kim DH. GABARAPs and LC3s have opposite roles in regulating ULK1 for autophagy induction. *Autophagy*. 2020;16:600-614. doi:10.1080/15548627.2019.1632620

77. Gottlieb RA, Andres AM, Sin J, Taylor DP. Untangling autophagy measurements: all fluxed up. *Circ Res*. 2015;116:504-514. doi:10.1161/CIRCRESAHA.116.303787

78. Koliopoulos MG, Lethier M, van der Veen AG, et al. Molecular mechanism of influenza a NS1-mediated TRIM25 recognition and inhibition. *Nat Commun*. 2018;9:1820. doi:10.1038/s41467-018-04214-8

79. Collier JJ, Suomi F, Olahova M, McWilliams TG, Taylor RW. Emerging roles of ATG7 in human health and disease. *EMBO Mol Med*. 2021;13:e14824. doi:10.15252/emmm.202114824

80. Koliopoulos MG, Esposito D, Christodoulou E, Taylor IA, Rittinger K. Functional role of TRIM E3 ligase oligomerization and regulation of catalytic activity. *EMBO J*. 2016;35:1204-1218. doi:10.15252/embj.201593741

81. Sanchez JG, Okreglicka K, Chandrasekaran V, Welker JM, Sundquist WI, Pornillos O. The tripartite motif coiled-coil is an elongated antiparallel hairpin dimer. *Proc Natl Acad Sci U S A*. 2014;111:2494-2499. doi:10.1073/pnas.1318962111

82. Carter SD, Mamede JI, Hope TJ, Jensen GJ. Correlated cryogenic fluorescence microscopy and electron cryo-tomography shows that exogenous TRIM5alpha can form hexagonal lattices or autophagy aggregates in vivo. *Proc Natl Acad Sci U S A*. 2020;117:29702-29711. doi:10.1073/pnas.1920323117

83. Di Rienzo M, Romagnoli A, Antonioli M, Piacentini M, Fimia GM. TRIM proteins in autophagy: selective sensors in cell damage and innate immune responses. *Cell Death Differ*. 2020;27:887-902. doi:10.1038/s41418-020-0495-2

84. Majolee J, Kovacevic I, Hordijk PL. Ubiquitin-based modifications in endothelial cell-cell contact and inflammation. *J Cell Sci*. 2019;132:jcs227728. doi:10.1242/jcs.227728

85. Qian Y, Wang Z, Lin H, et al. TRIM47 is a novel endothelial activation factor that aggravates lipopolysaccharide-induced acute lung injury in mice via K63-linked ubiquitination of TRAF2. *Signal Transduct Target Ther*. 2022;7:148. doi:10.1038/s41392-022-00953-9

86. Takase H, Hamanaka G, Ohtomo R, et al. Transcriptome profiling of mouse corpus callosum after cerebral Hypoperfusion. *Front Cell Dev Biol*. 2021;9:685261. doi:10.3389/fcell.2021.685261

87. Wang W, Xia Z, Farre JC, Subramani S. TRIM37 deficiency induces autophagy through deregulating the MTORC1-TFEB axis. *Autophagy*. 2018;14:1574-1585. doi:10.1080/15548627.2018.1463120

88. Pineda CT, Ramanathan S, Fon Tacer K, et al. Degradation of AMPK by a cancer-specific ubiquitin ligase. *Cell*. 2015;160:715-728. doi:10.1016/j.cell.2015.01.034

89. Han T, Guo M, Gan M, Yu B, Tian X, Wang JB. TRIM59 regulates autophagy through modulating both the transcription and the ubiquitination of BECN1. *Autophagy*. 2018;14:2035-2048. doi:10.1080/15548627.2018.1491493

90. Fan W, Liu T, Li X, et al. TRIM52: A nuclear TRIM protein that positively regulates the nuclear factor-kappa B signaling pathway. *Mol Immunol*. 2017;82:114-122. doi:10.1016/j.molimm.2017.01.003

91. Ma P, Schwarten M, Schneider L, et al. Interaction of Bcl-2 with the autophagy-related GABAA receptor-associated protein (GABARAP): biophysical characterization and functional implications. *J Biol Chem*. 2013;288:37204-37215. doi:10.1074/jbc.M113.528067

92. Ikeda R, Noshiro D, Morishita H, et al. Phosphorylation of phase-separated p62 bodies by ULK1 activates a redox-independent stress response. *EMBO J*. 2023;42:e113349. doi:10.15252/embj.2022113349

93. Fiorentini F, Esposito D, Rittinger K. Does it take two to tango? RING domain self-association and activity in TRIM E3 ubiquitin ligases. *Biochem Soc Trans*. 2020;48:2615-2624. doi:10.1042/BST20200383

SUPPORTING INFORMATION

Additional supporting information can be found online in the Supporting Information section at the end of this article.